Synergistic Multi-Enzyme Cascades Assembled on Modular Protein Scaffolds for Efficient PET Biorecycling

Yujia Zhang (张钰嘉)[1,2], Chongsen Li (李崇森)[1,2], Ehsan Hashimi[2], Enting Xu (许恩婷)[3], Xuemei Yang (杨雪梅)[3], Yanbing Lin (林雁冰)[1], Hui Gao (高辉)[2,*], Zhuobin Liang (梁卓斌)[2,*,+]

[1] College of Life Sciences, Northwest A&F University, Yangling, Shaanxi, 712100, China

[2] Institute of Molecular Physiology, Shenzhen Bay Laboratory, Shenzhen, Guangdong, 518132, China

[3] School of Science, Harbin Institute of Technology (Shenzhen), Shenzhen, Guangdong, 518055, China

[+] Lead Contact

[*] Correspondence addressed to: ZL (zbliang@szbl.ac.cn) or HG (gaohui@szbl.ac.cn)

Abstract

The global crisis of polyethylene terephthalate (PET) waste demands new strategies for sustainable management. Biocatalytic recycling offers a promising route, but direct depolymerization under moderate conditions is often limited by kinetic constrains of individual enzyme. Here, we engineer and optimize modular protein scaffolds that utilize orthogonal interaction domains, including the cohesin-dockerin pairs from bacterial cellulosomes and the SH3 ligand/domain pair from mouse Crk, to assemble complementary hydrolases (PETase, MHETase, and ICCG) into a synergistic multi-enzyme cascade. This architecture overcomes intermediate inhibition, efficiently converting PET hydrolysis products into the final monomers, terephthalic acid (TPA) and ethylene glycol (EG), outperforming previous multi-enzyme systems. The system's application is further evaluated by stability enhancement via immobilization on metal-organic frameworks (MOFs), coupling depolymerization to the valorization of EG into glycolic acid (GA), and adapting the system for scalable whole-cell biocatalysis. This scaffold-based multi-enzyme approach provides a new strategy for developing integrated biocatalytic systems to advance a circular PET economy.

Main

Polyethylene terephthalate (PET), a ubiquitous polyester valued for its durability and versatility, poses a major sustainability crisis due to its environmental persistence and the limitations of traditional recycling. Its vast global production, exceeding 30 million tons annually, leads to widespread plastic pollution, harming terrestrial and marine ecosystems [1], releasing hazardous microplastics [2], and posing risks to human health [3]. Traditional mechanical recycling requires extensive sorting, often yields low-value products due to incomplete degradation [4], and can further exacerbate microplastic pollution [5]. Chemical recycling routes such as methanolysis and glycolysis, while promising, typically require high-temperature operations and the complex purification steps to isolate the final products [6,7].

Biocatalytic degradation, harnessing enzymes from microorganisms to break down PET polymers, has been proposed as an alternative strategy [8]. This approach is attractive due to its potential for complete degradation, lower environmental impact, and the generation of valuable products through recycling and upcycling, as showcased in early-phase industrial demonstrations [9]. Several PET hydrolases, including TfH [10], leaf-branch cutinase (LCC) [11], and *Is*PETase [12], have been identified and further engineered [13,14] (**Supplementary Table 1**). However, existing biocatalytic systems still face major hurdles such as incomplete monomer production [15], intermediate inhibition [16], limited efficiency on high-crystallinity PET, and cost-effectiveness [17], hindering their widespread industrial implementation.

Recent efforts to address these limitations have focused on multi-enzyme systems that leverage the complementary action of different PET hydrolases [18–20] (**Supplementary Table 2**). While free enzyme mixtures successfully alleviate intermediate accumulation, their synergistic efficiency is constrained by stochastic diffusion and a lack of precise spatial organization [19-20]. Conversely, while direct genetic fusions successfully enforce spatial proximity [18], these static single-chain architectures are structurally challenging to expand or modify. Consequently, current approaches generally lack the structural modularity required to easily substitute enzyme variants, integrate additional functional modules, and readily adapt the cascade for diverse applications like monomer upcycling and whole-cell catalysis.

To address these challenges, here we engineer a modular, self-assembling multi-enzyme system, inspired by the natural cellulosome architect. This system enables the precise co-localization of multiple hydrolases, creating a synergistic complex that overcomes the kinetic bottlenecks of individual enzymes. We term this system the Scaffold-enabled PET Enzyme Ensemble-augmented Degradation platform (SPEED). We report the iterative design and optimization of the system, followed by demonstrations of its industrial relevance through enhanced stability via immobilization, direct coupling of depolymerization to monomer valorization, and adaptation for whole-cell biocatalysis. This work establishes a scaffold-based framework for engineering efficient, multi-step biocatalytic pathways for PET plastic recycling and upcycling.

Results

Synergistic enzyme-scaffold system for enhanced PET degradation

To harness the complementary properties of different PET hydrolases, we designed a multi-enzyme system based on the two-step PET hydrolysis pathway (**Fig. 1a**). Building on previous work that demonstrated the synergy of combining PETase and MHETase [18], we selected FAST-PETase [14] (FAST) for its high catalytic activity and MHETase [12] for its ability to convert inhibitory intermediates bis-(2-hydroxyethyl) terephthalate (BHET) and mono-(2-hydroxyethyl) terephthalate (MHET) into the final monomers, terephthalic acid (TPA) and ethylene glycol (EG).

Inspired by natural cellulosomes [21,22], we engineered and purified dockerin-fused versions of these enzymes to self-assemble onto cohesin-containing scaffolds, Scaf.1 and Scaf.2 (**Supplementary Fig. 1** and **2**), forming Complex-A and Complex-B, respectively (**Fig. 1b**). Scaf.2 includes a carbohydrate-binding module (CBM) [23] to enhance affinity for the PET substrates, which was confirmed in a binding assay (**Fig. 1c**). Isothermal titration calorimetry (ITC) further verified the binding of both MHETase-CelF and FAST-PETase-CelK to the Scaf.2 scaffold (**Fig. 1d**,**e**).

PET biodegradation assays confirmed the functional synergy of the assembled complexes in hydrolyzing PET substrates of varying crystallinity. These substrates, including PET powder, a low-crystallinity PET film (film-L), and a high-crystallinity PET film (film-H), sourced from suppliers common to the field and their crystallinity were further characterized by differential scanning calorimetry to ensure comparability with previous work (**Supplementary Fig. S3**). While combining free FAST and MHETase enhanced degradation compared to FAST alone, assembling them onto the scaffolds further boosted performance (**Fig. 1f-h**). Complex-B (using Scaf.2 with a CBM module) slightly outperformed Complex-A, yielding 22.11 mM (PET powder), 17.29 mM (film-L), and 0.73 mM (film-H) total products after 96 hours.

While these results are consistent with the synergy benefit reported in an earlier dual-enzyme fusion system [18], our modular scaffold provides the structural flexibility required to expand the multi-enzyme cascade and achieve improved degradation performance (**Supplementary Table 2** and **File 1-2**).

Optimization of MHETase expression, assembly, and activity

Despite the above validated benefits of MHETase, the relatively low expression of recombinant MHETase in *E. coli* hindered further development. To address this bottleneck, we pursued a multi-pronged optimization strategy focusing on host strain selection, induction expression conditions, codon usage, and protein domain fusions, that improved MHETase expression and purification in *E. coli* (**Fig. 2a**, **Supplementary Fig. 4** and **5**). We replaced its fused CelF dockerin with a Src Homology 3 (SH3) peptide ligand ($SH3_L$) and redesigned the scaffold (Scaf.3) to include the corresponding SH3 domain ($SH3_D$) from the mouse Crk protein [24] for assembly (**Fig. 2b**). We discovered that the fusion topology was critical for this new interaction: an N-terminal fusion of the $SH3_L$ to optiMHETase resulted in high-affinity binding to Scaf.3 (K_D = 12.6 nM), whereas a C-terminal fusion abrogated binding entirely (**Fig. 2c**,**d**). This optimized N-terminal construct achieved an ~ 80-fold enhancement in binding affinity over the original CelF dockerin-based system (**Fig. 2c**

vs. **Fig. 1d**), and was comparable to the FAST-PETase-CelK interaction with Scaf.3 (**Fig. 2e**). These successful modifications enabled the assembly of the improved Complex-C (**Fig. 2b**).

Degradation assays across various PET substrates revealed significant improvements (**Fig. 2f-h**). Complex-C yielded 22.37 mM, 23.22 mM and 0.83 mM TPA production with PET powder, film-L and film-H, respectively. This represents a 3-fold increase over FAST-only groups and a 22.2% average increase over Complex-B (**Fig. 2f-h** vs. **Fig. 1f-h**). These results confirm Complex-C's effectiveness in promoting PET recycling.

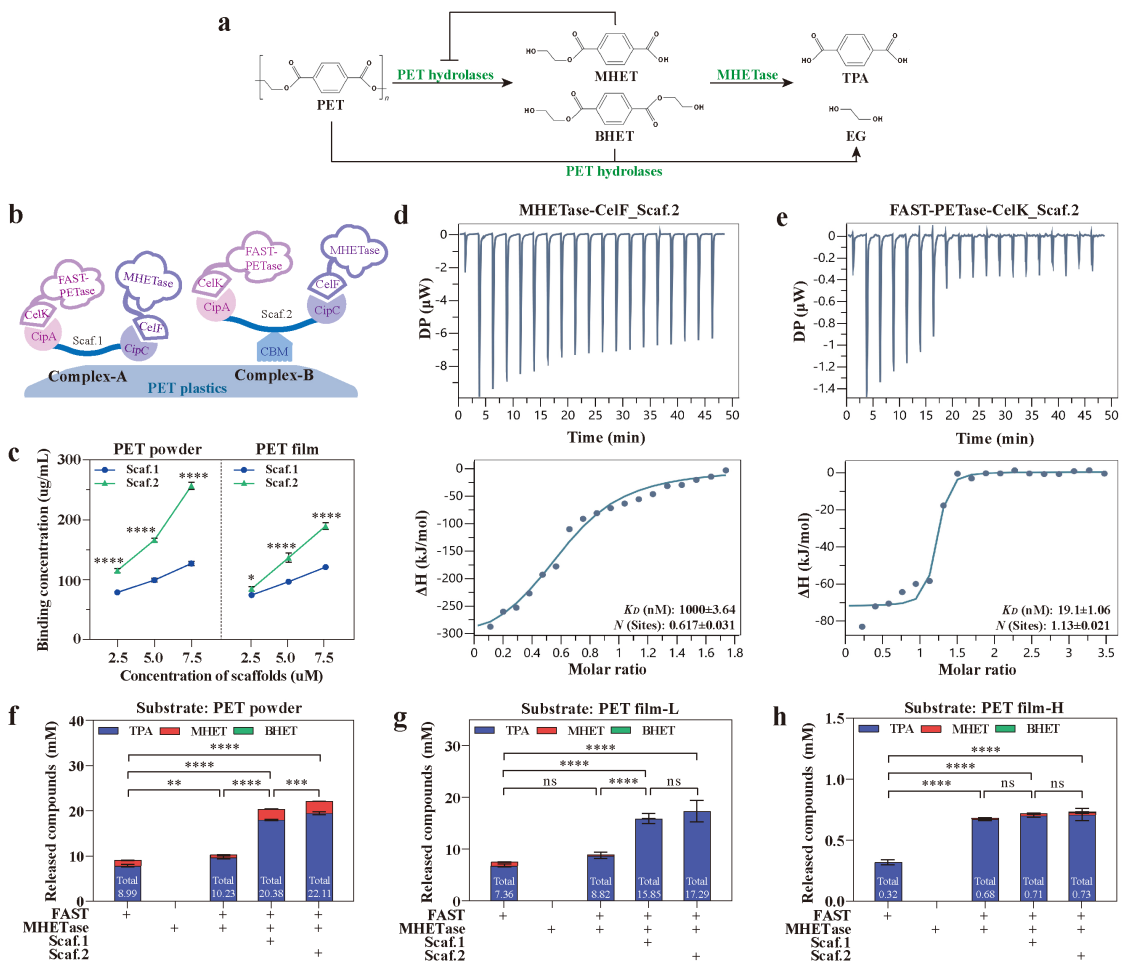

Fig. 1: Scaffold assembly of PET hydrolases enhances depolymerization. a Schematic of the two-step PET hydrolysis pathway. PET is hydrolyzed by PET hydrolases to intermediates (MHET, BHET), which are subsequently converted to monomers (TPA, EG) by MHETase. **b** Schematic of the initial scaffold design. Dockerin-fused enzymes self-assemble onto cohesin-containing scaffolds to form Complex-A (Scaf.1) and Complex-B (Scaf.2). CelF/CipC: orthogonal dockerin/cohesin from *Clostridium cellulolyticum*; CelK/CipA: orthogonal dockerin/cohesin from *Clostridium thermocellum*. **c** Binding assay showing the affinity of Scaf.1 and Scaf.2 for PET powder and film substrates. **d**, **e** Isothermal titration calorimetry (ITC) confirms the binding of MHETase-CelF (**d**, K_D = 1000 nM) and FAST-PETase-CelK (**e**, K_D = 19.1 nM) to Scaf.2. **f–h** PET degradation assays comparing free enzymes (FAST, MHETase) with scaffolded complexes (Complex-A, Complex-B) on PET powder (**f**), low-crystallinity film (film-L) (**g**), and high-crystallinity film (film-H) (**h**). Reactions contained 100 mg PET, 0.1 nmol of each enzyme with an enzyme:scaffold molar ratio of 0.2:1, were incubated at 30 °C, pH 7.0, for 96 h. Data are presented as mean ± s.d. (n = 3). Statistical significance was determined by one-way ANOVA (ns, not significant; $P < 0.05$, $^{*}P < 0.01$, $^{**}P < 0.001$, $^{***}P < 0.0001$).

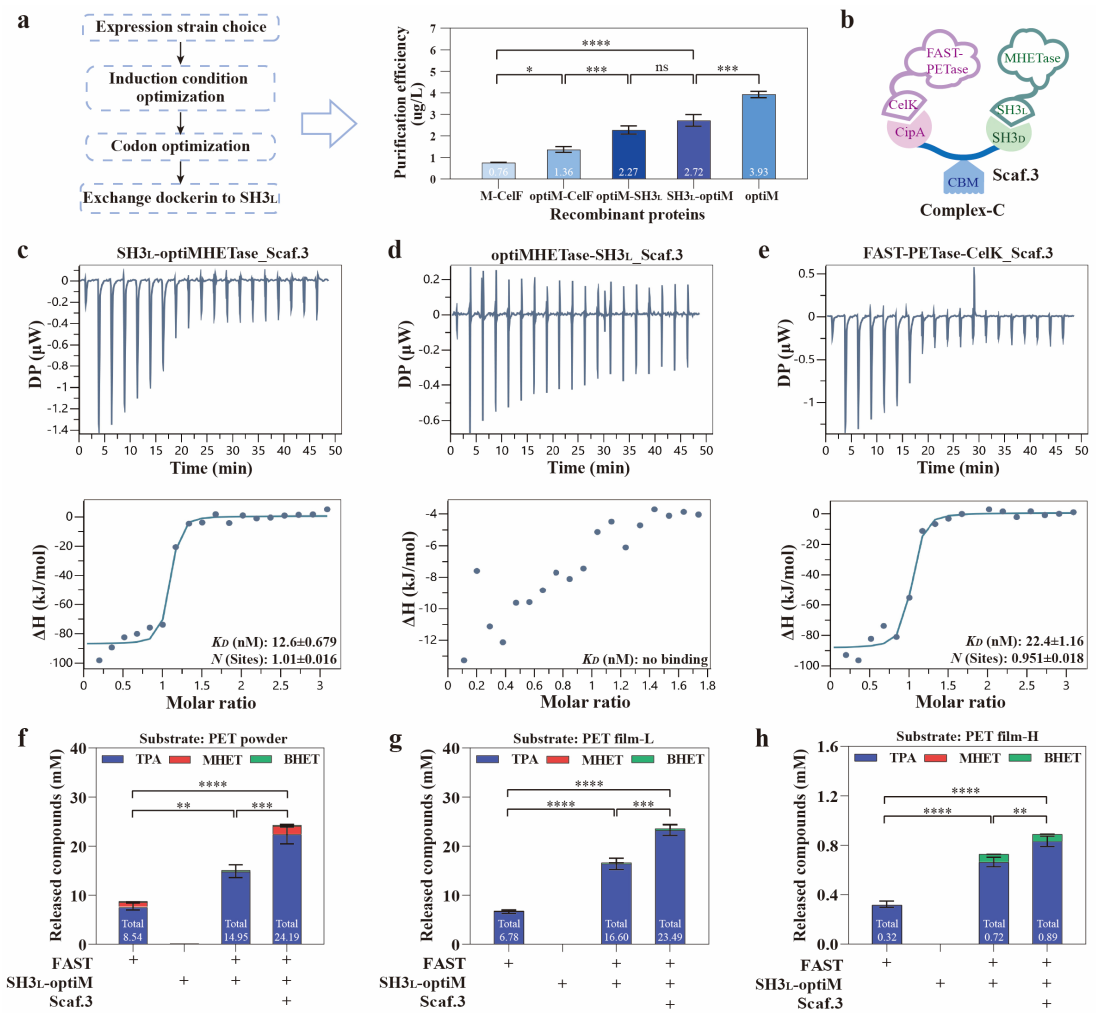

Fig. 2: Optimization of MHETase enhances scaffold assembly and complex activity. a Schematic illustration of MHETase optimization strategy and the resulting purification efficiency of different MHETase variants from selected *E. coli* C41(DE3) strain with optimal induction condition (16 °C with 1 mM IPTG for 18 h). Purification efficiency is defined as the final yield of purified protein (ug) from each liter (L) of *E. coli* cultures with similar OD (cell density). M-CelF: MHETase-CelF; optiM-CelF: codon optimized M-CelF; M-optiSH3$_L$: optiMHETase-SH3$_L$; SH3$_L$-optiM: SH3$_L$-optiMHETase; optiM: codon optimized MHETase (as control). **b** Schematic of the redesigned Complex-C, assembled on the Scaf.3 (CipA-CBM-SH3$_D$). SH3$_D$/SH3$_L$: SH3 domain sourced from the mouse protein Crk and its cognate peptide ligand. **c-e** ITC binding analysis of SH3$_L$-optiMHETase **(c)**, optiMHETase-SH3$_L$ **(d)**, and FAST-PETase-CelK **(e)** to the redesigned scaffold Scaf.3. **f-h** PET degradation assays comparing individual enzymes, enzyme mixtures, and the fully assembled Complex-C (FAST + SH3$_L$-optiM + Scaf.3), on PET powder **(f)**, film-L **(g)**, and film-H **(h)**. SH3$_L$, SH3 ligand; SH3$_D$, SH3 domain. Reactions contained 100 mg PET, 0.1 nmol of each enzyme with an enzyme:scaffold molar ratio of 0.2:1, were incubated at 30 °C, pH 7.0, for 96 h. Data are presented as mean ± s.d. (n = 3). Statistical significance was determined by one-way ANOVA (ns: not significant, *p < 0.1, **p < 0.01, ***p < 0.001, ****p < 0.0001).

141 **Modular scaffold expansion to boost PET degradation capacity**

142 The transition from Complex-A to Complex-C demonstrates the modularity of the SPEED design,
143 allowing for tailored enzyme combinations for diverse substrates. To broaden substrate range, we
144 next incorporated ICCG, an enzyme active towards higher-crystallinity substrates (6%-40%) [25],
145 complementing the preference of FAST-PETase for lower-crystallinity PET plastics (1%-30%) [14].
146 Using the dockerin-cohesin pair ScaA-ScaB [26], ICCG was integrated into a new scaffold, CipA-
147 CBM-$SH3_D$-ScaB (Scaf.4), forming Complex-D (**Fig. 3a** and **Supplementary Fig. 6**).

148 Degradation assays revealed several key insights (**Fig. 3b-d**). The result showed ICCG has
149 slightly higher activity towards PET substrates compared to FAST at 30 °C. The inclusion of
150 MHETase with ICCG led to near-complete conversion of MHET and BHET intermediates into TPA,
151 and EG by implication. Moreover, combining ICCG, FAST, and MHETase greatly increased TPA
152 productions to 33.07 mM (powder), 36.09 mM (film-L) and 0.93 mM (film-H). Scaf.4 further
153 increased the efficiency to 44.66 mM (powder), 49.03 mM (film-L) and 1.32 mM (film-H). Finally,
154 we confirmed the strong binding of all three enzymes (FAST, MHETase, and ICCG) to the scaffold,
155 demonstrating stability of Complex-D (**Fig. 3e-g**). Overall, Complex-D further enhanced PET
156 biodegradation efficiency and achieved high intermediate conversion.

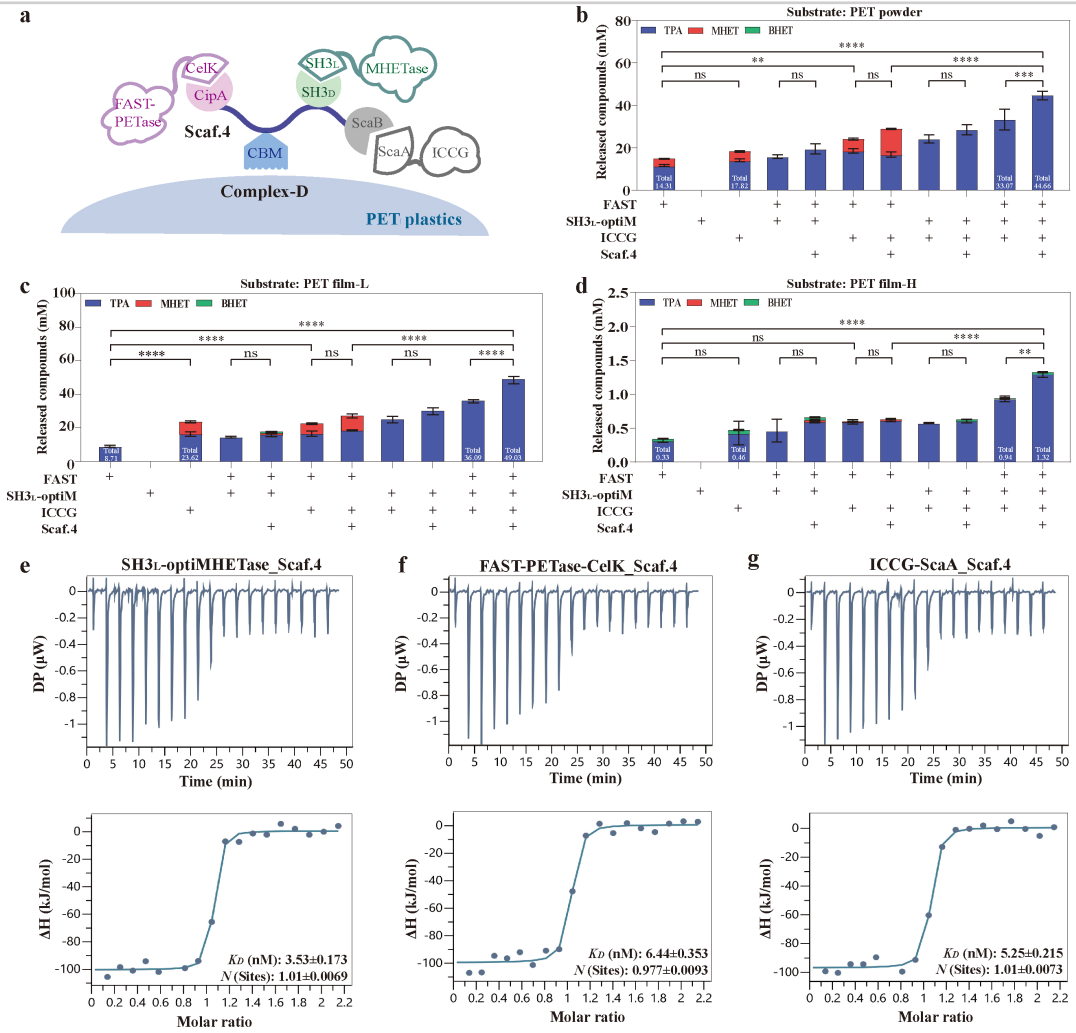

Fig. 3: A three-enzyme scaffolded cascade improves PET degradation and monomer purity. a Schematic of the expanded three-enzyme complex (Complex-D), incorporating FAST-PETase, optiMHETase, and ICCG on the modular Scaf.4 scaffold. ScaA/ScaB: orthogonal dockerin/cohesin pair from *Ruminococcus flavefaciens*. **b-d** PET degradation assays on PET powder (**b**), film-L (**c**), and film-H (**d**) comparing individual enzymes, enzyme mixtures, and the fully assembled Complex-D (FAST + SH3L-optiM + ICCG + Scaf.4). Reactions contained 100 mg PET, 0.1 nmol of each enzyme with an enzyme:scaffold molar ratio of 0.2:1, were incubated at 30 °C, pH 7.0, for 96 h. **e-g** ITC confirms tight binding of all three enzymes to Scaf.4: SH3L-optiMHETase (**e**, K_D = 3.53 nM), FAST-PETase-CelK (**f**, K_D = 6.44 nM), and ICCG-ScaA (**g**, K_D = 5.25 nM). Data are presented as mean ± s.d. (n = 3). Statistical significance was determined by one-way ANOVA (ns: not significant, *p < 0.1, **p < 0.01, ***p < 0.001, ****p < 0.0001).

168 **Improve SPEED performance through reaction optimization**

169 To optimize the performance of the three-enzyme Complex-D and improve enzyme cost-
170 effectiveness, we systematically investigated its PET degradation efficiency under various reaction
171 conditions (**Fig. 4a**), beginning with the impact of enzyme-scaffold ratio (**Fig. 4b**). While increasing
172 enzyme concentration could enhance product release (**Fig. 4b**, bar graph), ratios exceeding 0.5:1
173 (enzyme:Scaf.4) led to diminishing benefits from the scaffold (**Fig. 4b**, dot graph and
174 **Supplementary Fig. 7**). This suggests that at higher concentrations, the scaffold becomes saturated,
175 and the surplus of free enzyme does not contribute to the synergistic effect, reducing the overall cost-
176 effectiveness. Consequently, we adopted the 0.5:1 enzyme-to-scaffold ratio for subsequent
177 optimizations.

178 Next, we investigated the influence of temperature and pH on Complex-D performance (**Fig.**
179 **4c**,**d**). While previous findings indicate optimal temperatures for free FAST and ICCG are
180 approximately 40 °C and 60 °C, respectively [27], our results for the complex showed that increasing
181 the temperature above 40 °C led to an accumulation of intermediates and reduced TPA production,
182 likely due to adverse effects on the less thermostable MHETase (**Supplementary Fig. 8**).
183 Consequently, the highest total product yield (176.40 mM, with 174.71 mM as TPA) was achieved at
184 40 °C and pH 7.0, conditions consistent with the optimum for MHETase activity [28].

185 To directly assess the impact of scaffolding on enzyme kinetics, we compared the performance
186 of the scaffold-binding enzymes against their free counterparts (**Supplementary Fig. 9**). These
187 results showed that while the optimal reaction temperature and pH did not change upon scaffold
188 binding, the scaffolded FAST and ICCG, but not MHETase, exhibited both higher PET degradation
189 efficiency and increased tolerance to sub-optimal conditions, such as elevated pH and temperature.

190 In addition, the robustness of Complex-D under these optimal conditions was validated across
191 diverse PET substrates, including PET powder, films of low and high crystallinity, and post-consumer
192 commercial bottles (**Supplementary Fig. 10**). The system demonstrated significantly enhanced
193 degradation activity across all tested materials over the controls, achieving conversion to the final
194 monomer.

195 Finally, the catalytic stability and substrate versatility of the optimized Complex-D were further
196 assessed through long-term PET degradation experiments (**Fig. 4e-g**). The complex exhibited robust
197 and sustained hydrolysis across all PET substrates over 17 days. It is noteworthy that these optimized
198 conditions, which balance the kinetics of the three-enzyme cascade, also allow robust performance
199 of the free enzyme mixture, though its activity remained lower than that of the scaffolded complex.
200 Scanning electron microscopy (SEM) confirmed this enhanced activity, revealing that treatment with
201 the optimized Complex-D induced significantly greater surface erosion on PET film and a more
202 pronounced reduction in PET powder particle size after 96 hours compared to the individual enzymes
203 (**Fig. 4h** and **Supplementary Fig. 11**).

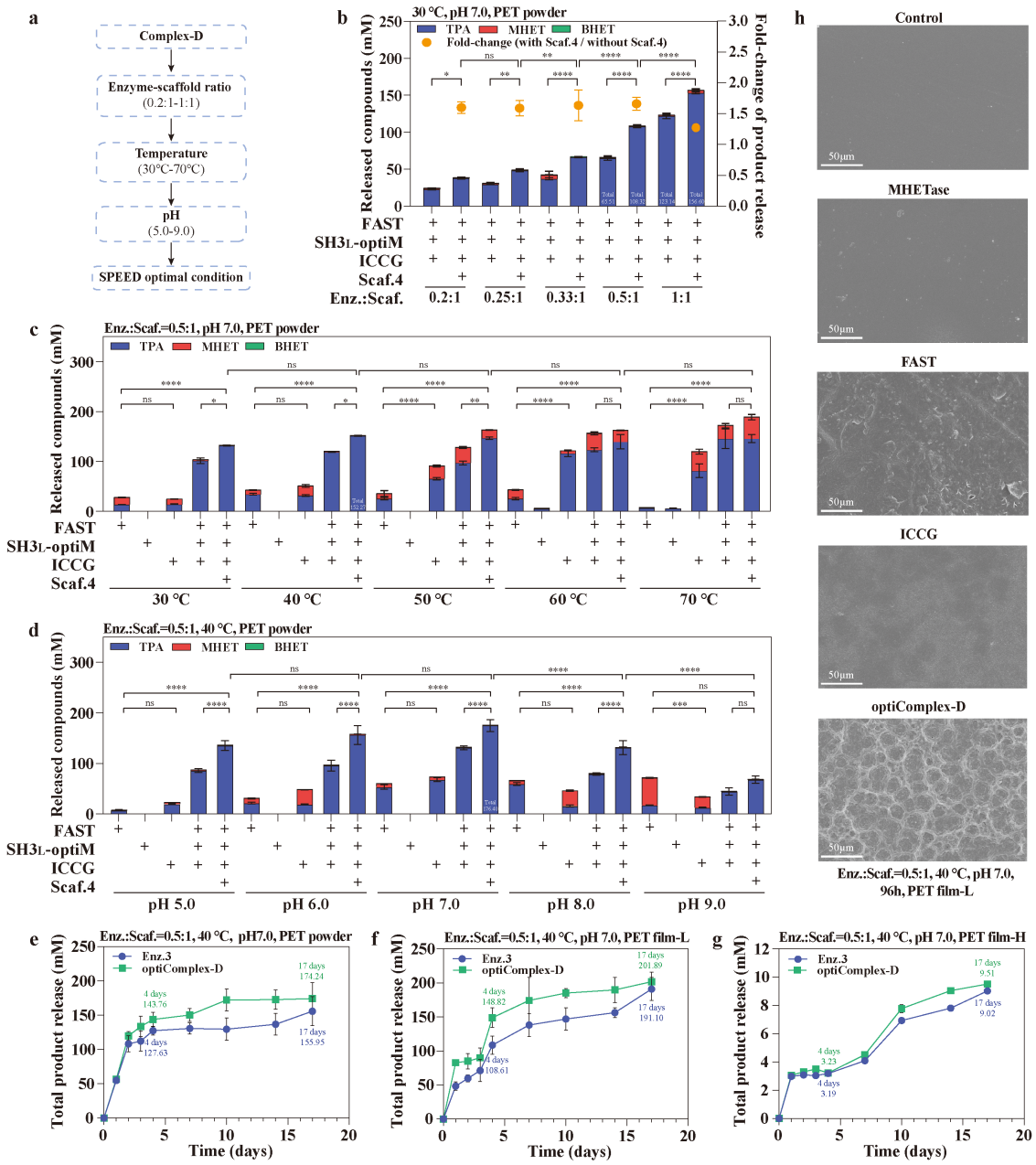

Fig. 4: Reaction optimization enhances performance of the three-enzyme complex. a Strategy for optimizing Complex-D reaction conditions. **b** Effect of the enzyme:scaffold molar ratio on total product release from PET powder (bars, left axis) and the fold-change in activity conferred by the scaffold (dots, right axis). An optimal ratio of 0.5:1 was selected. Reactions contained 100 mg PET powder, enzymes with a constant 1 μM scaffold, were incubated at 30 °C, pH 7.0, for 96 h. **c** Influence of temperature on PET degradation efficiency and final products (0.5:1 enzyme:scaffold ratio, pH 7.0, 96 hours, 100 mg PET powder). **d** Impact of pH on PET degradation efficiency and final products (0.5:1 enzyme:scaffold ratio, 40 °C, 96 h, 100 mg PET powder). **e-g** Long-term (17-day) degradation time-course analysis for optiComplex-D vs. a non-scaffolded enzyme mixture (Enz.3) on PET powder (**e**), film-L (**f**), and film-H (**g**) under 40 °C, pH 7.0, with 0.5:1 enzyme:scaffold ratio. **h** Scanning electron microscopy (SEM) images of film-L after 96 hours of treatment at 40 °C, pH 7.0, with no enzyme (Control), single enzyme (MHETase, FAST, ICCG), and optiComplex-D. Data are presented as mean ± s.d. (n = 3). Statistical significance was determined by one-way ANOVA (ns: not significant, *p < 0.1, **p < 0.01, ***p < 0.001, ****p < 0.0001).

Tailored MOF immobilization enhances catalytic stability and reusability

To improve the system's stability and reusability for potential industrial translation, we explored enzyme immobilization strategies. We first immobilized optiComplex-D onto the metal-organic framework ZIF-8 [29], selected for its favorable properties including low cost and tunable properties [30,31]. Because balancing enzyme stability and substrate accessibility is a critical in heterogeneous biocatalysis, so we prepared three distinct configurations: (i) surface immobilization, (ii) incomplete encapsulation, and (iii) full encapsulation (**Fig. 5a** and **Supplementary Fig. 12**).

As expected, catalytic activity was highly dependent on substrate access. The fully encapsulated complex (iii) showed minimal PET degradation, while the incompletely encapsulated (ii) and surface-immobilized (i) complexes both demonstrated catalytic activity, with the former showing the highest performance (**Fig. 5b**). Furthermore, ZIF-8 immobilization significantly improved the complex's stability across a wider pH and temperature range (**Supplementary Fig. 13**). The scaffold's synergistic function remained crucial post-immobilization, with scaffolded complexes outperforming non-scaffolded enzyme mixtures in long-term assays (**Fig. 5c**). Reusability was also improved, as the top-performing complex retained over 53 % of its initial activity after four 4-day cycles, substantially outperforming the ~ 30 % retained by the free complex (**Fig. 5d** and **Supplementary Fig. 14**).

To benchmark our MOF-based approach, we also immobilized the complex on calcium phosphate (CaP) nanocrystals, a versatile biomaterial that can be used for enzyme immobilization [32,33] (**Supplementary Fig. 15a**). While the initial 4-day product yield of optiComplex-D@CaP was comparable to that of the ZIF-8 system (**Supplementary Fig. 15b** vs. **Fig. 5c**), the CaP matrix proved less robust in metrics critical for practical application. For instance, the ZIF-8 system demonstrated enhanced reusability, retaining over 53 % of its activity after four cycles, compared to 40.9 % for the CaP-immobilized complex (**Fig. 5d** vs. **Supplementary Fig. S15c**). Furthermore, ZIF-8 offered a wider operational window. While the thermal stability of both systems was limited by the enzymes themselves, the ZIF-8 immobilized complex retained a greater proportion of its activity at 70 °C compared to the CaP system (**Supplementary Fig. 13a**,**c** vs. **14d**). The inherent chemical instability of CaP led to its dissolution and loss of activity at pH below 6.0 (**Supplementary Fig. 15e**), a limitation not observed with the ZIF-8 matrix. We also noted that the optiComplex-D@CaP formulation was unstable during cold storage, releasing the enzyme complex over time.

Together, these findings demonstrate that a tailored immobilization strategy using ZIF-8 preserves the catalytic advantages of the scaffolded architecture while conferring the enhanced stability and reusability beneficial for industrial translation.

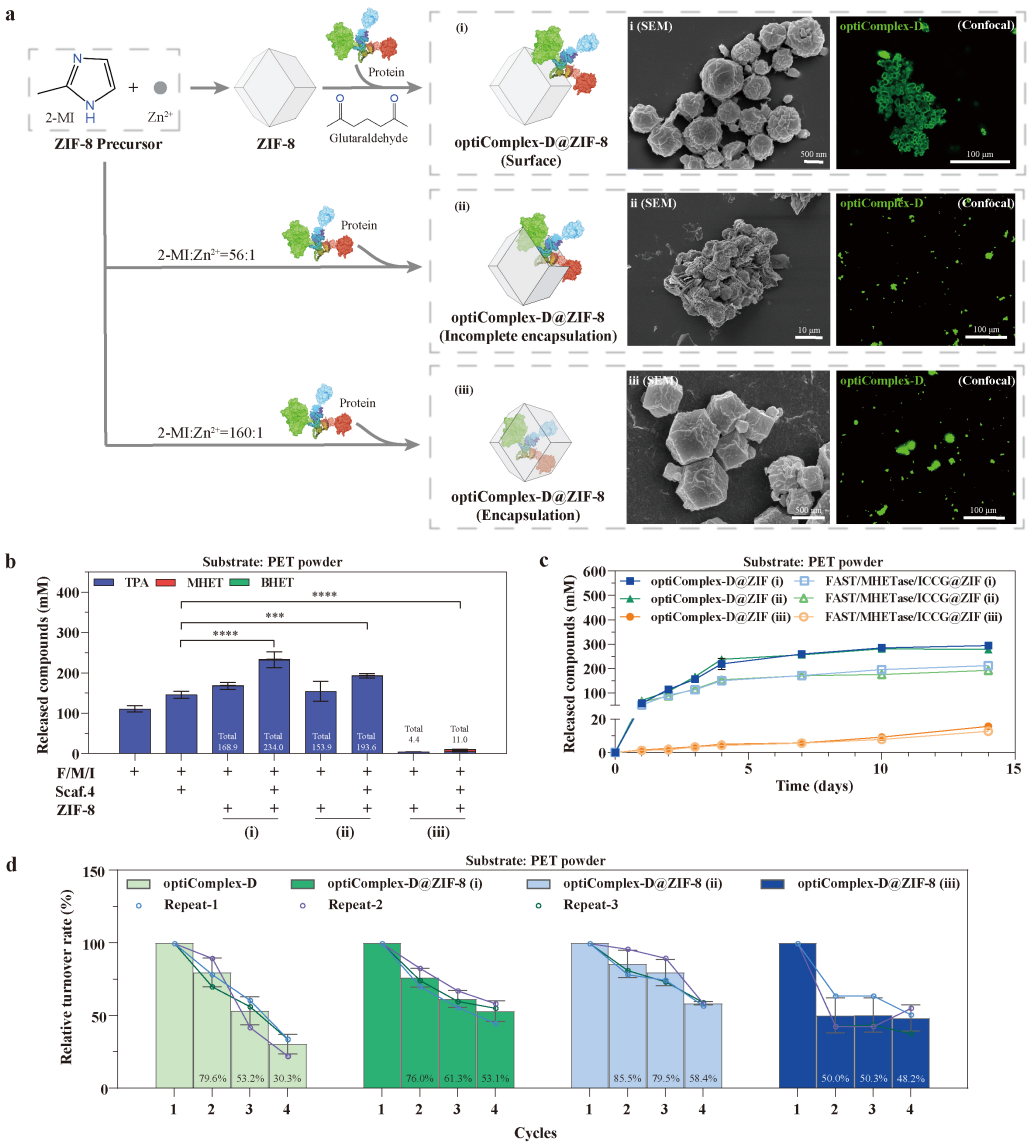

Fig. 5: ZIF-8 immobilization enhances complex stability and reusability. a Schematic of three ZIF-8 immobilization strategies: (i) surface immobilization via glutaraldehyde crosslinking, (ii) incomplete encapsulation using a 2-MI:Zn^{2+} ratio of 56:1, and (iii) full encapsulation using a 160:1 ratio, following an established protocol [34]. Successful immobilization and the distinct morphology of each configuration were confirmed by SEM and fluorescence microscopy. 2-MI, 2-methylimidazole. Alexa Fluor® 488 conjugated anti-His antibody was used to detect His-tagged proteins. The loading efficiency of optiComplex-D@ZIF-8 was 75.26 % (i), 85.95 % (ii), 91.13 % (iii) respectively. **b** Total product yield after 96 h on PET powder comparing three immobilization configurations. **c** Long-term (14-day) activity of scaffolded (optiComplex-D) and non-scaffolded (F/M/I) enzymes immobilized in the three configurations. **d** Reusability of free vs. immobilized optiComplex-D over four 4-day cycles. Reactions were performed at 40 °C, pH 7.0, with 100 mg PET powder, 0.25 nmol enzymes in a 0.5:1 enzyme:scaffold ratio. Data are presented as mean ± s.d. (n = 3). Statistical significance was determined by one-way ANOVA (ns: not significant, *p < 0.1, **p < 0.01, ***p < 0.001, ****p < 0.0001).

262 **PET upcycling through scaffold-mediated biocatalysis**

263 The modularity of the SPEED platform allows for the integration of PET depolymerization with
264 downstream valorization pathways [35–37]. To evaluate this capability, we engineered a second multi-
265 enzyme assembly, Complex-E, designed to convert the PET degradation product ethylene glycol (EG)
266 to glycolic acid (GA) [38], a versatile C2 platform chemical. GA has direct applications in dermatology
267 and cosmetics and also serves as the monomer for poly(lactide-co-glycolide acid) (PLGA)-a high-
268 performance biodegradable polymer used to create absorbable surgical sutures and drug delivery
269 systems [39–41]. This synthetic pathway employs the sequential action of 1,2-propanediol
270 oxidoreductase (FucO) [42] and glycolaldehyde dehydrogenase (AldA) [38], with *Lactobacillus reuteri*
271 NADH oxidase (LrNox) [35] regenerating the required NAD^+ cofactor, a similar strategy building upon
272 our prior work [43] (**Fig. 6a,b**).

273 We evaluated GA production by comparing sequential and simultaneous reaction schemes. A
274 sequential approach, where Complex-E was added after a 96-hour PET degradation, yielded 2.65
275 mM GA (**Fig. 6c**). In contrast, a simultaneous, one-pot reaction with both complexes yielded 4.61
276 mM of GA in the same total time, a 1.74-fold increase (**Fig. 6d**). This enhanced performance likely
277 stems from the continuous conversion of EG, improving the overall pathway flux. The importance
278 of the scaffold in orchestrating this complex cascade was evident. When the upcycling enzymes
279 (FucO, AldA, LrNox) were added as free proteins alongside optiComplex-D, PET degradation was
280 significantly inhibited (**Fig. 6e**, compare bars 4 and 7). This result suggests that the free enzymes
281 competed for binding sites on the Scaf.4 scaffold, disrupting the depolymerization cascade. Thus,
282 assembling enzymes for each stage into distinct, scaffolded complexes is crucial for one-pot
283 efficiency. This tandem reaction demonstrates the application of the SPEED design principle for
284 engineering complex, multi-step biocatalytic processes.

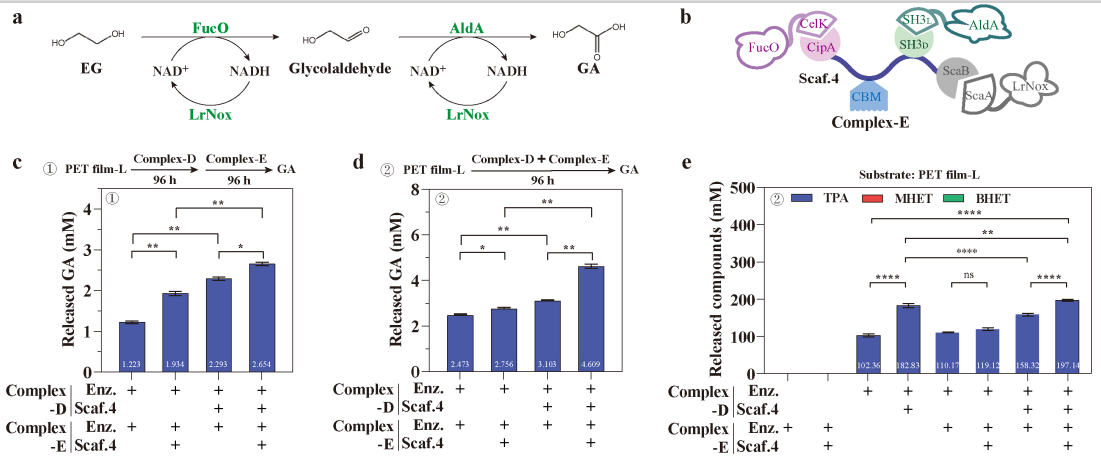

Fig. 6: Modular scaffolds for one-pot PET depolymerization and monomer upcycling. a The upcycling cascade converts EG to glycolic acid (GA) via a three-enzyme pathway with NAD^+ regeneration. **b** Schematic of the upcycling enzyme complex (Complex-E). **c** GA production in a sequential reaction, where Complex-E is added after a 96 h PET degradation step. **d** GA production in a simultaneous, one-pot reaction containing both Complex-D and Complex-E from the start, showing a 1.74-fold improvement over the sequential approach. **e** PET degradation performance under different enzyme and scaffold combinations. All reactions were performed at 40 °C, pH 7.0, for 96 hours, with 0.25 nmol of each individual enzyme and enzyme:scaffold molar ratios of 0.5:1 for optiComplex-D and 1:1 for Complex-E. Data are presented as mean ± s.d. (n = 3). Statistical significance was determined by one-way ANOVA (ns: not significant, *p < 0.1, **p < 0.01, ***p < 0.001, ****p < 0.0001).

SPEED platform adapted for whole-cell biocatalysis

To demonstrate the SPEED platform's potential for scalable biorecycling, we adapted it for a whole-cell biocatalyst system using yeast surface display, which avoids costly enzyme purification steps. In our system, an engineered yeast strain displays the cohesin scaffold on its cell surface, a second strain was engineered to secrete the dockerin-fused hydrolases (FAST-PETase and MHETase) into the medium (**Fig. 7a**). We selected the industrial yeast *Pichia pastoris* SMD1168 for its high-density growth and protein secretion capabilities [44,45] (**Supplementary Fig. 16**), and the scaffold was displayed to the cell surface using the SED1 anchor protein, which demonstrated the highest efficiency among several candidates (**Fig. 7b**). We also confirmed the high copy numbers of the expression cassettes in the engineered strains (**Supplementary Table 3**).

Co-culturing these two strains resulted in the spontaneous, self-assembly of the enzyme complex onto the yeast cell surface, which was confirmed by confocal microscopy and flow cytometry (**Fig. 7c**,**d**) though we could not observe the individual enzyme on SDS-PAGE. We then compared the PET degradation efficiency of this whole-cell system against a control culture containing only the enzyme-secreting strain (without the scaffold-displaying yeast). The surface-displayed SPEED complex exhibited a 3.05-fold higher PET degradation activity than the secreted enzymes alone (**Fig. 7e**). This result demonstrates that the scaffold-mediated proximity and synergy are maintained in a complex *in vivo* environment, providing a promising proof-of-concept for developing robust, industrially relevant live cell systems for PET recycling.

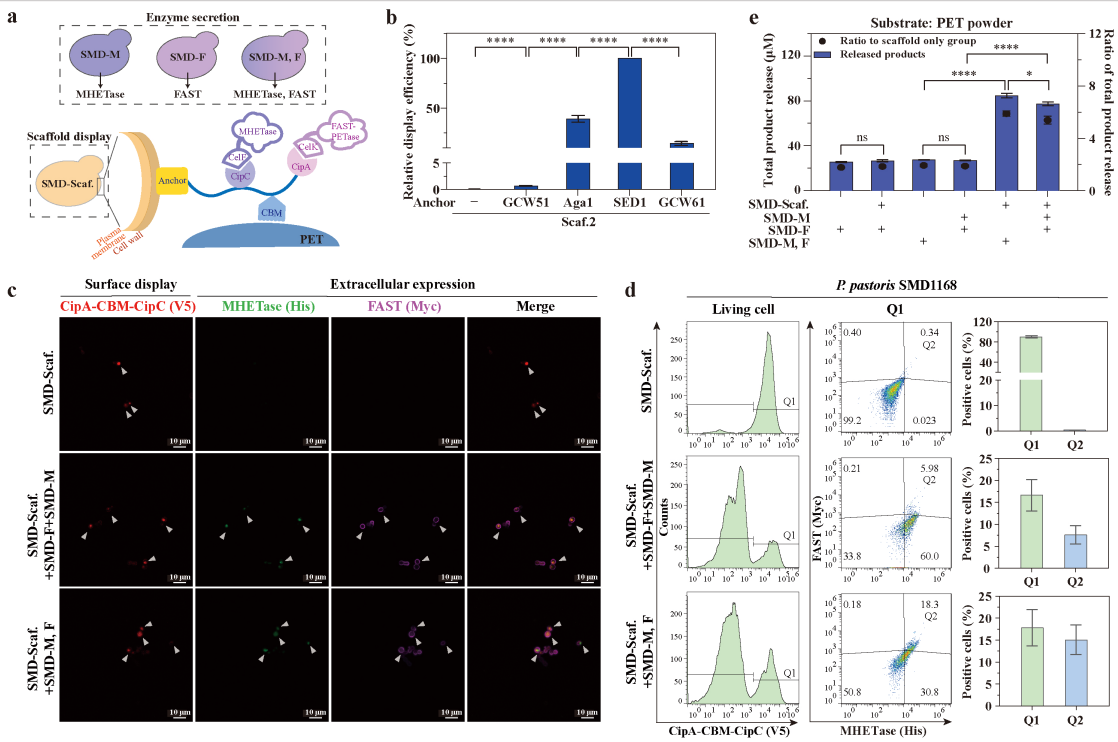

Fig. 7: SPEED-enabled live cell system for PET degradation. a Design of the co-culture system in *P. pastoris*, where one strain displays the cohesin scaffold and a second strain secretes dockerin-fused enzymes for self-assembly on the cell surface. **b** Screening of anchor proteins for scaffold display, identifying SED1 as the most efficient. **c**, **d** Confocal microscopy (**c**) and flow cytometry (**d**) confirm the co-localization of secreted enzymes (MHETase-His, FAST-Myc) on the surface of scaffold-displaying yeast (Scaf.-V5). **e** PET degradation assays showing that the co-culture system with the scaffold-displayed complex significantly outperforms the control culture containing only free, secreted enzymes. Reactions used 100 mg PET powder and were incubated for 48 h at 30 °C, pH 7.0 after a 96-h protein expression induction. The ratio of enzyme-secreting strains to the scaffold-displaying strain was 10:1. Data are presented as mean ± s.d. (n = 3). Statistical significance was determined by one-way ANOVA (ns: not significant, *p < 0.1, **p < 0.01, ***p < 0.001, ****p < 0.0001).

Discussion

In this study, we constructed a modular protein scaffold platform for PET biorecycling by assembling multi-enzyme cascades via orthogonal cohesin-dockerin and SH3 ligand/domain interactions. This spatial organization addresses the kinetic limitations observed in non-scaffolded enzyme mixtures by facilitating substrate channeling, thereby mitigating the accumulation of inhibitory intermediates (MHET, BHET) and increasing conversion to the final monomers (TPA, EG). We further evaluated the platform's modularity through three proofs-of-concept directed toward potential industrial translation: immobilizing the complex on metal-organic frameworks to improve catalytic stability and enzyme reusability; extending the cascade to couple depolymerization with ethylene glycol upcycling; and adapting the assembly for a scalable live-cell system via yeast surface display (**Fig. 8**).

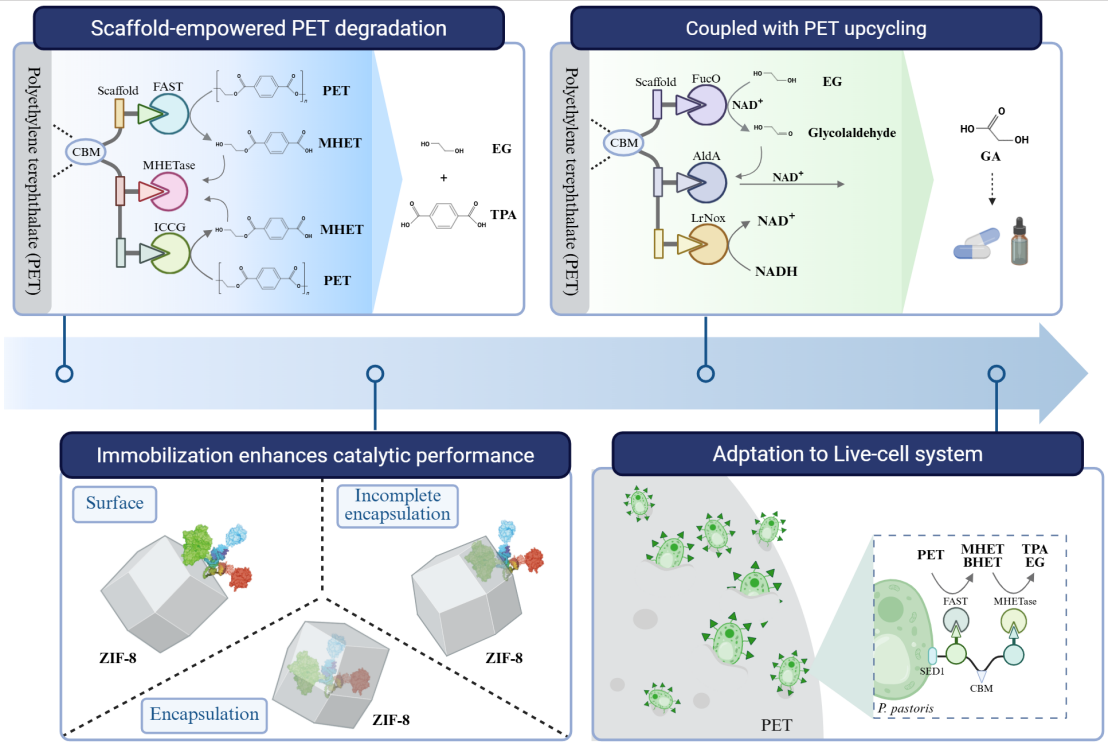

Fig. 8: Schematic summary of the PET biorecycling system reported in this study. Top left: the scaffold-mediated PET degradation cascade. Bottom left: structural configurations for anchoring the enzyme complex onto metal-organic frameworks. Top right: coupling of the system to convert the ethylene glycol monomer into glycolic acid. Bottom right: assembly of the biocatalytic system via yeast surface display.

Building on previous multi-enzyme strategies, this scaffold-mediated assembly improved the product yield per mole of enzyme (**Supplementary Table 2**). Regarding substrate conversion extents (**Supplementary Table 4**), the optiComplex-D degraded 16.40% of high-crystallinity (40.82%) PET powder after four days. Immobilization on ZIF-8 increased this 4-day conversion to 27.14%. Over an extended 14-day reaction, the immobilized complexes achieved conversion extents of 33.49% for the high-crystallinity powder (40.82%) and 36.72% for a lower-crystallinity (17.99%) PET film.

These conversion extents reflect the use of untreated substrates, representing distinct experimental parameters from studies reporting near-complete depolymerization. For example,

Tournier *et al*. utilized amorphized PET, higher enzyme loading, and a pH-stat bioreactor to chemically drive the reaction equilibrium [13]. Similarly, Lu *et al*. evaluated post-consumer products with initial crystallinity ranging from 1.2% to 6.24% [14]. Rather than maximizing bulk conversion via substrate pretreatment or continuous reactor optimization, this study evaluates normalized catalytic efficiency and targeted monomer production on untreated, high-crystallinity materials. These data indicate that structural scaffolds facilitate monomer production on PET substrates.

While this study describes a scaffold-mediated platform for PET biorecycling, further research is necessary for industrial translation. The current experiments were not evaluated under high-solids loading conditions, and techno-economic analyses are required to determine cost-effectiveness. Future development should focus on integrating thermally and chemically stable enzymes to broaden the operational parameters, as well as expanding the available upcycling pathways to establish viable biorefining routes. In summary, the modularity and scaffold-mediated spatial organization evaluated in this work provide a framework for constructing biocatalytic systems for plastic waste conversion.

364 ## Methods

365 **Plasmid construction**

366 Genes encoding enzymes and scaffolds were commercially synthesized (Tsingke, China), with all
367 key primer sequences used in this study provided in **Supplementary Table 5.** Standard cloning
368 techniques were employed using *E. coli* DH5α. Briefly, FAST-PETase (FAST), ICCG, FucO, AldA,
369 LrNox and scaffold variants were cloned into pET28a vectors, while MHETase constructs utilized
370 pET28a and pColdII vectors. Synthesized genes and pET28a vectors were digested with NdeI and
371 XhoI (37 °C, 1h), followed by T4 DNA ligase-mediated ligation (25 °C, 2h). This generated plasmids
372 pET28a-FAST-PETase-CelK, pET28a-MHETase-CelF, pET28a-ICCG-ScaA, pET28a-FucO-CelF,
373 pET28a-$SH3_L$-AldA, pET28a-LrNox-ScaA, pET28a-CipA-CBM-CipC, pET28a-CipA-CBM-$SH3_D$,
374 and pET28a-CipA-CBM-$SH3_D$-ScaB. In enzyme-scaffold complexes, enzymes were fused with
375 native dockerin from cellulase enzyme CelK [46] and CelF [47] to construct FAST-PETase-CelK, FucO-
376 CelF and MHETase-CelF, respectively. Meanwhile, the corresponding cohesin CipA and CipC were
377 tethered together to form scaffold protein CipA-CipC (Scaf.1). Scaf.1 incorporates an additional
378 carbohydrate-binding module (CBM) from *Clostridium thermocellum* [23,48], a module that enhances
379 protein affinity for PET substrates [49], to form CipA-CBM-CipC (Scaf.2). The protein-protein
380 interaction pair $SH3_L$-$SH3_D$ [24] and doc-coh pair ScaA-ScaB [26] were used to construct $SH3_L$-AldA,
381 CipA-CBM-$SH3_D$ (Scaf.3), CipA-CBM-$SH3_D$-ScaB (Scaf.4), $SH3_L$-optiMHETase, ICCG-ScaA,
382 LrNox-ScaA, respectively.

383 To construct the live-cell PET degradation system, *Pichia pastoris* SMD1168 was employed.
384 The pPIC9K vector was utilized for the insertion and expression of MHETase, and Scaf.3. To
385 engineer strain with exogenous gene insertion, primer pairs pScf-F/pScf-R were employed to amplify
386 CipA-CBM-CipC-SED1, while primer pairs pF-F/pF-R and pM-F/pM-R were utilized to amplify
387 FAST and MHETase, respectively. Additionally, primers pPIC9K-F/pPIC9K-R were used to amplify
388 pPIC9K linearized vector. The pPICZC vector was utilized for the insertion of MHETase. MHETase
389 and pPICZC linearized vector were amplified using primer pairs pZM-F/pZM-R and pPICZC-
390 F/pPICZC-R. The linearized gene and vector were connected by seamless cloning to form the
391 expression vectors pPICZC-FAST, pPIC9K-MHETase, pPIC9K-CipA-CBM-CipC-SED1, and
392 pPICZC-MHETase. The expression vectors were linearized by SacI digestion and transformed into
393 *P. pastoris* SMD1168. The transformants were cultured in histidine-deficient (SD-his) plates and
394 screened for strains with high copies of the exogenous gene insertion by SD-his plates containing 5
395 mg/mL G418.

396 To reposition $SH3_L$ from the C-terminus to the N-terminus of optiMHETase, sequential PCR
397 was performed with primer pairs M1-F/M-R, M2-F/M-R, and M3-F/M-R. To remove $SH3_L$ from
398 $SH3_L$-optiMHETase (as control), PCR was performed with primer pairs M1-F/Md-R. For C-terminal
399 His-tag of MHETase, PCR was conducted using primers his-F/his-R. Subsequent digestion with NdeI
400 and XbaI, followed by T4 DNA ligase-mediated recombination, generated plasmids pColdII-
401 MHETase-CelF, pColdII-optiMHETase-CelF, pColdII-optiMHETase-$SH3_L$, pColdII-$SH3_L$-

402 optiMHETase, and pColdII-optiMHETase. All protein constructs were designed with both N- and C-
403 terminal His tags.

404 **Recombinant protein expression and purification**

405 For Recombinant protein expression, *E. coli* C41 (DE3) cells were transformed with pColdII-based
406 plasmids, while *E. coli* BL21 (DE3) and *E. coli* Rosetta (DE3) cells were used for pET28a constructs.
407 Transformants were grown in LB media supplemented with appropriate antibiotics (100 μg/mL
408 ampicillin for pColdII, 500 μg/mL kanamycin for pET28a) at 37 °C until OD_{600} reached 0.6-0.7.
409 IPTG (0.5 mM or 1.0 mM final concentration for MHETases, 1.0 mM for others) induced expression
410 overnight (at 16 °C or 37 °C for MHETases, 16 °C for others). Cells were harvested by centrifugation
411 and stored at -80 °C.

412 Cells were resuspended in lysis buffer (50 mM sodium phosphate, 300 mM NaCl, pH 8.0),
413 disrupted by sonication, and the supernatant was collected by centrifugation. HisTrap HP column
414 purification employed an ÄKTA pure system (Cytiva, China). Bound protein was washed with 85 %
415 binding buffer (20 mM sodium phosphate, 30 mM imidazole, 500 mM NaCl, pH 7.4) with 15 %
416 elution buffer (20 mM sodium phosphate, 500 mM imidazole, 500 mM NaCl, pH 7.4) and eluted
417 with a linear gradient of 15-100 % elution buffer. Eluates were concentrated (Amicon Ultra, Merck
418 Millipore, China), buffer-exchanged to 50 mM sodium phosphate (SP buffer, pH 7.0), and assessed
419 for purity/concentration by NanoDrop™ One/One^{C} (Thermo Fisher, U.S.A.). The high purity of all
420 proteins was confirmed by SDS-PAGE (**Supplementary Fig. S1**), and representative FPLC
421 purification profiles are shown in **Supplementary Fig. S2**. Proteins were stored in storage buffer
422 (50 % glycerol in SP buffer, pH 7.0) at -80 °C.

423 **Binding assay of protein scaffolds to PET**

424 Following previously established protocols [49], PET powder (crystalline, Xing-xiang new materials,
425 China) or PET film (amorphous, Goodfellow, UK) were washed with 10 % SDS, water, and SP buffer
426 (pH 7.0). CipA-CipC (Scaf.1) or CipA-CBM-CipC (Scaf.2) were incubated at 2.5, 5, and 7.5 μM
427 with 100 mg PET powder in 200 μL SP buffer (pH 7.0) overnight at 4 °C. Samples were centrifuged
428 (12000 g, 1 min), washed twice with SP buffer (pH 7.0), and residual protein in solution was
429 quantified using a BCA Protein Quantification Kit (Yeason, China). Binding protein concentration
430 was calculated as follows (C, concentration; before, before incubation with PET; after, after
431 incubation with PET):

432 $$Binding\ protein\ concentration = C_{(before)} - C_{(after)}$$

433 **Binding assay of enzymes to scaffolds**

434 Enzyme-scaffold protein interactions were analyzed by MicroCal PEAQ-ITC Automated (Malvern
435 Panalytical, Netherland). Enzymes were placed in the reaction cell, and scaffold protein titrations
436 were performed at 25 °C with 18 injections of 2 μL substrate [50]. Heats generated by dilution were
437 corrected, and data were analyzed using the MicroCal PEAQ-ITC Analysis Software (one set of sites
438 model).

439 For live-cell system, flow cytometry was used to analyze enzyme-scaffold protein interactions.
440 After a 96-hour induction at 30 °C, the yeast cells were collected by centrifugation at 4000 g for 10
441 min at 4 °C, then washed and diluted with DPBS. Subsequently, 1×10^7 cells and 0.1 μL of each
442 antibody (V5 tag antibody, Invitrogen 451098; His tag antibody, Cell Signaling Technology 14930;
443 or Myc tag antibody, R&D Systems IC3696P) were incubated for 45 min, washed and detected
444 through flow cytometry.

445 **Characterization of crystallinity of PET substrates**

446 Thermal crystallinity of PET substates was determined by differential scanning calorimetry (DSC
447 8000, PerkinElmer) (**Supplementary Fig. 3**). PET substrates (75 μm powder; low crystallinity PET
448 film, film-L; high crystallinity PET film, film-H; Nongfu Spring water bottle, NFbottle) were heated
449 from 30 °C to 300 °C at a heating rate of 30 °C/min, kept at 300 °C for 1 min, and then cooled to 0 °C
450 at 5 min with same rate of 30 °C/min [14,49]. The theoretical heat of melting value (ΔHm°) of 100 %
451 crystallized PET was 140.1 J/g. Percentage crystallinity was calculated with the heat of melting
452 (ΔHm) and cold crystallization (ΔHc) values, as the following equation:

453 $$Crystallinity\ (\%) = \frac{\Delta Hm - \Delta Hc}{\Delta \mathrm{Hm}^\circ} \times 100\%$$

454 **Synthesis and characterization of MOF-immobilized enzyme complexes**

455 For synthesis of FAST/MHETase/ICCG/Scaffold@ZIF-8 (optiComplex-D@ZIF-8) and
456 FAST/MHETase/ICCG@ZIF-8, a certain amount of proteins (0.25 nmol individual enzyme of FAST,
457 MHETase and ICCG with/without scaffold to form enzyme complexes), an aqueous solution of 2-
458 methylimidazole (790 mM, 1.75 mL for incompletely encapsulated crystals, 5 mL for completely
459 encapsulated crystals) and 0.25 mL $Zn(NO_3)_2\cdot6H_2O$ (97.5 mM) were stirred at 500 g for 5 min. To
460 synthesize ZIF-8, 1.75 mL 2-MI (790 mM) and 0.25 mL $Zn(NO_3)_2\cdot6H_2O$ (97.5 mM) was stirred.
461 Subsequently, the mixture was left undisturbed for 3 h at 4 °C [34]. For synthesis of enzyme complexes
462 immobilization on ZIF-8 carrier, 20 mg prepared ZIF-8 with a certain amount of proteins was cultured
463 in 5 mL SP buffer containing 50 mM glutaraldehyde at 4 °C for 3 h [51]. Finally, the prepared
464 Enz.Scaf@ZIF-8, Enz@ZIF-8 and ZIF-8 were collected by centrifugation at 3500 g for 10 minutes
465 and dispersed into 0.5 mL SP buffer.

466 For characterizations, confocal microscopy images were recorded by Nikon confocal laser
467 scanning microscope; SEM (ZEISS GeminiSEM 300) were used to measure the immobilized samples.

468 **Synthesis and characterization of CaP-immobilized enzyme complexes**

469 The FAST/MHETase/ICCG@CaP and FAST/MHETase/ICCG/Scaffold@CaP (optiComplex-
470 D@CaP) were synthesized according to the previously reported method with slight modification by
471 mixing solution I with solution II [52,53]. For solution I, 1 mg $Ca_3(PO_4)_2$ was added to 2 mL of 50 mM
472 sodium phosphate buffer with different pH. For solution II, 0.25 nmol individral enzymes
473 with/without 0.5 nmol scaffold (Scaf.4) were added to 2 mL of 100 mM $CaCl_2$ solution. Solution I
474 and II were balanced for 1 h at 4 °C, respectively, then mixed with equal volume. After incubation
475 for 12 h at 4 °C, the precipitate was washed thrice and dispersed into 0.5 mL SP buffer to obtain
476 optiComplex-D@CaP and FAST/MHETase/ICCG@CaP. For characterizations, confocal

477 microscopy images were recorded by Nikon confocal laser scanning microscope.

478 **Loading efficiencies of enzymes in ZIF-8 and CaP**

479 The loading efficiencies of compatible enzymes in ZIF-8 and CaP were evaluated with BCA Protein
480 Quantification Kit (Yeason, China). Specifically, collecting the supernatant from the washing process
481 and final step synthesis of enzyme@ZIF-8 or enzyme@CaP, then detecting the concentration and
482 volume of the supernatant. The loading efficiencies were then determined as the ratio of embedded
483 enzymes amount to the initial amount of enzymes [34], which was calculated based on the following
484 equation ($m_{(before)}$, the initially added enzyme amount (mg); $C_{(after)}$, the enzyme concentration in the
485 supernatant (mg/mL); $V_{(after)}$, the volume of supernatant (mL)):

486 $$Loading\ efficiency\ (\%) = \frac{m_{(before)} - C_{(after)}V_{(after)}}{m_{(before)}} \times 100\%$$

487 **Exogenous gene insertion analysis**

488 The insertion copy number of exogenous genes was determined by quantitative real-time PCR
489 (qPCR), following an established protocol [44]. The genomic DNA of engineered *P. pastoris* SMD1168
490 was extracted by the Yeast Genomic DNA Extraction Kit (TIANGEN, DP307). Genomic DNA of *P.*
491 *pastoris* $SMD1168_{His4::CipA\text{-}CBM\text{-}CipC\text{-}SED1}$, *P. pastoris* $SMD1168_{His4::FAST}$, *P. pastoris*
492 $SMD1168_{His4::MHETase}$ and *P. pastoris* $SMD1168_{His4::FAST\text{-}MHETase}$ were used as templates, respectively,
493 for the amplification of the genes CipA-CBM-CipC, FAST, MHETase with the primer pairs qC-
494 F/qC-R, qF-F/qF-R, and qM-F/qM-R; the housekeeping gene GAPDH was amplified with the primer
495 pairs qGAPDH-F/qGAPDH-R to obtain the copy number of the exogenous protein inserted in the
496 engineered strains. All primer sequences were listed in **Supplementary Table 3**.

497 **Establishment and characterization of live-cell PET biodegradation system**

498 For live-cell systems, surface-displaying and secretory-expressing engineered yeast strains were
499 individually pre-cultured in BMGY (1 % yeast extract, 2 % peptone, 100 mM potassium phosphate
500 buffer, 1.34 % amino acid-free yeast nitrogen source, and 1 % (v/v) glycerol, pH 6.0) at 30 °C for 12
501 h, after which the number of cells was measured in the pre-cultured products. *P. pastoris*
502 $SMD1168_{His4::enzyme}$ was mixed with *P. pastoris* $SMD1168_{His4::scaffold}$ in a 10:1 ratio, resulting in a
503 final system comprising 2×10^7 *P. pastoris* $SMD1168_{His4::scaffold}$. The expression medium BMMY (1%
504 yeast extract, 2 % peptone, 100 mM potassium phosphate buffer, 1.34 % amino acid-free yeast
505 nitrogen, and 1 % (v/v) methanol, pH 6.0) was employed for protein expression and enzyme-scaffold
506 assembly. Expression was conducted at 30 °C, with the medium augmented with 0.5 % methanol at
507 24-hour intervals over a period of 96 hours.

508 Confocal microscopy images and flow cytometry assays were recorded by Nikon confocal laser
509 scanning microscope. His Tag Alexa Fluor® 488-conjugated Antibody (IC0501G, R&D Systems),
510 V5 Tag Monoclonal Antibody (451098, Invitrogen), Human c-Myc PE-conjugated Antibody
511 (IC3696P, R&D Systems) to detect MHETase and/or FAST with His tag, FAST with Myc tag,
512 scaffold with V5 tag, respectively.

513 For surface displaying assays mediated by different anchors, displaying efficiency was
514 calculated with median florescence intensity (MFI) and copy number by flow cytometry and qPCR,
515 as the following equation:

516 $$Relative\ display\ efficiency = \frac{MFI_{V5\ positive}}{Copy\ number\ of\ the\ scaffold}$$

517 **Degradation assay of PET plastics**

518 Standard reactions contained 100 mg PET (powder, low or high crystallinity PET films), 0.2 μM
519 individual enzyme, 500 μL reaction buffer (50 mM sodium phosphate, 0.5 mM $CaCl_2$, 10 % DMSO,
520 pH 7.0). For complex assembly, enzymes (0.2 μM) were pre-mixed with scaffold (1 μM) for 40 min
521 at 25 °C. Unless otherwise stated, degradations proceeded for 96 h at 30 °C.

522 To optimize the enzyme:scaffold ratio within SPEED, ratios ranged from 0.2:1 to 1:1 (constant
523 scaffold protein 1 μM). Effects of pH (5.0-9.0, 30 °C), temperature (30-70 °C, pH 7.0), and PET
524 substrate type (PET powder, low and high crystallinity PET films, commercial bottle) were also
525 analyzed.

526 For PET upcycling reaction, PET degrading enzymes (FAST, MHETase, ICCG) were combined
527 with Scaf.4 (1 μM, CipA-CBM-$SH3_D$-ScaB) in an optimized ratio. Similarly, the upcycling enzymes
528 (FucO, AldA, LrNox), which facilitate the synthesis of valuable products from PET, were mixed with
529 Scaf.4 (0.5 mM) in a molar ratio of 1:1. The mixed proteins were incubated at 25 °C for 40 minutes
530 to achieve complex assembly. Following assembly, the upcycling complex was incorporated into the
531 PET degradation product, which was reacted for four days under optimal conditions. Alternatively,
532 the PET degradation complex was mixed with the upcycling complex and 100 mg PET Film-L for
533 further conversion. The reactions were conducted in 500 μL systems for 2 to 4 days in SP buffer
534 (with 1 mM additional NAD^+).

535 For live-cell PET degradation, a mixture of 1×10^9 induced *Pichia pastoris* SMD1168 was
536 collected, then placed in 400 μL of sterile glycine-NaOH buffer (pH 7.0) containing 100 mg PET
537 powder to facilitate the degradation reaction. The degradation reaction was conducted at 30 °C for
538 48 h. All reactions were terminated at 95 °C for 10 min, supernatants were 0.22 μm filtered, and
539 released products were quantified by HPLC (High Performance Liquid Chromatography).

540 **MHETase degradation assay**

541 To assess the intermediates degradation ability of MHETase, 0.5 μM $SH3_L$-optiMHETase was
542 combined with 5 mM MHET and BHET in 500 μL reaction buffer (50 mM sodium phosphate, 0.5
543 mM $CaCl_2$, 10 % DMSO, pH 7.0). The reactions were constructed at varying temperatures (30 °C,
544 40 °C, 50 °C, 60 °C, 70 °C) for 96 h and terminated by heating to 95 °C for 10 min. Supernatants
545 were 0.22 μm filtered, and released products were quantified by HPLC.

546 **HPLC analysis**

547 TPA, MHET, BHET and GA, standards were obtained from Aladdin (China). The analysis of the
548 samples was conducted using an Agilent 1260 LC system equipped with G1315A diode array
549 detector (DAD) and ZORBAX StableBond C18 column (4.6×150 mm, 5 μm, Agilent) for TPA,

MHET and BHET detection, as well as a refractive index detector (RID) and a Xtimate® Sugar-H column (3.8×300 mm, 5 μm, Welch Materials) for GA detection.

For TPA, MHET and BHET detection, the mobile phase consisted of 0.1 % formic acid (A) and acetonitrile (B); separation used a flow rate of 1 mL/min (80 % A / 20 % B, 10 min); detection was performed at 240 nm, 25 ℃ with C18 column [25].

For GA detection, the mobile phase consisted of 5 mM H_2SO_4 (Solvent as ddH_2O); separation used a flow rate of 1 mL/min (15 min); detection was performed at 80 ℃ with Sugar-H column. Analyte concentrations were determined using calibration curves (10-500 mM). Samples were adaptively diluted with ultrapure water prior to analysis.

Scanning electron microscopy (SEM)

Low-crystallinity PET film (6 mm diameter) and PET powder samples were analyzed by SEM (HuaSuan Technolygy, China) after degradation (40 ℃, 96 h, pH 7.0). Samples were washed (10 % SDS, water, ethanol), dried, gold-coated, and imaged.

Scaffold-enzyme structural prediction

In this study, three enzymes structures were obtained from the Protein Data Bank (https://www.rcsb.org/. FAST-PETase: 6IJ6, MHETase: 6QZ4, ICCG: 8JMP, CelK: 3P6B, $SH3_L$: 1PRM, ScaA: 5N5P). The structure of the scaffold was predicted by AlphaFold2. After running the standard AlphaFold2 MSA generation pipeline against UniRef, MGnify, PDB, and BFD, the sequence with highest pLDDT greater than 0.9 is chosen as the final model prediction. The depiction of enzyme-scaffold complex was visualized by BioRender (https://www.biorender.com/).

Statistical analysis

One-way analysis of variance (ANOVA) followed by normality test was employed to evaluate the significance of differences among different treatments. Unless specify, total products were used for the significance test. Statistical analysis were conducted using GraphPad Prism 9.0 software. ns: not significant, *$p < 0.1$, **$p < 0.01$, ***$p < 0.001$, ****$p < 0.0001$.

Declaration of Competing Interest

Z.L, Y.Z. and H.G. are inventors on two granted patents filed by Shenzhen Bay Laboratory (CN118754996B, CN118754951B) that cover enzyme complexes and engineered *P. pastoris* systems and their uses for plastics biodegradation relating to this work. Other authors have no potential competing interests to declare.

Data Availability

All data are available in the main text, supplementary information and **Source Data**. Additional information related to this study is available from the corresponding author upon reasonable request.

Acknowledgements

This study was supported by funding from the Shenzhen Bay Laboratory Startup Fund, the Shenzhen Outstanding Talents Training Fund, the National Natural Science Foundation of China (Grant Numbers: 32471546), Shenzhen Research Funding for Postdocs and the Key Research and Development Program of Shaanxi Province, China (Grant Numbers: 2022NY-055 and 2019NY-187). We acknowledge the intellectual and experimental contributions of all authors for this study and its manuscript preparation. We are particularly grateful for the insights gained from discussions with lab members in the Zhuobin Liang and Yanbin Lin labs. We would like to acknowledge Ziwei Luo for her technical assistance in the illustration of Figure. 1. We also extend our gratitude to the Haizhen Long and Jianchuan Wang lab at Shenzhen Bay Laboratory for their assistance in experiment setup. Finally, we thank the Research Core Facility of Shenzhen Bay Laboratory for their technical support, especially for the use of ÄKTA and HPLC instruments.

References

1. Lau, W. W. Y. *et al.* Evaluating scenarios toward zero plastic pollution. *Science* **369**, 1455–1461 (2020).
2. Xu, C. *et al.* Are we underestimating the sources of microplastic pollution in terrestrial environment? *J Hazard Mater* **400**, 123228 (2020).
3. Gao, R., Pan, H., Kai, L., Han, K. & Lian, J. Microbial degradation and valorization of poly(ethylene terephthalate) (PET) monomers. *World J Microbiol Biotechnol* **38**, 89 (2022).
4. Ragaert, K., Delva, L. & Van Geem, K. Mechanical and chemical recycling of solid plastic waste. *Waste Management* **69**, 24–58 (2017).
5. Suzuki, G. *et al.* Global discharge of microplastics from mechanical recycling of plastic waste. *Environmental Pollution* **348**, 123855 (2024).
6. Uekert, T. *et al.* Technical, Economic, and Environmental Comparison of Closed-Loop Recycling Technologies for Common Plastics. *ACS Sustain Chem Eng* **11**, 965–978 (2023).
7. Qureshi, M. S. *et al.* Pyrolysis of plastic waste: Opportunities and challenges. *J Anal Appl Pyrolysis* **152**, 104804 (2020).
8. Kushwaha, A., Goswami, L., Singhvi, M. & Kim, B. S. Biodegradation of poly(ethylene terephthalate): Mechanistic insights, advances, and future innovative strategies. *Chemical Engineering Journal* **457**, 141230 (2023).
9. Amalia, L., Chang, C.-Y., Wang, S. S.-S., Yeh, Y.-C. & Tsai, S.-L. Recent advances in the biological depolymerization and upcycling of polyethylene terephthalate. *Curr Opin Biotechnol* **85**, 103053 (2024).
10. Müller, R., Schrader, H., Profe, J., Dresler, K. & Deckwer, W. Enzymatic Degradation of Poly(ethylene terephthalate): Rapid Hydrolyse using a Hydrolase from *T. fusca*. *Macromol Rapid Commun* **26**, 1400–1405 (2005).
11. Sulaiman, S. *et al.* Isolation of a Novel Cutinase Homolog with Polyethylene Terephthalate-Degrading Activity from Leaf-Branch Compost by Using a Metagenomic Approach. *Appl Environ Microbiol* **78**, 1556–1562 (2012).
12. Yoshida, S. *et al.* A bacterium that degrades and assimilates poly(ethylene terephthalate). *Science* **351**, 1196–1199 (2016).
13. Tournier, V. *et al.* An engineered PET depolymerase to break down and recycle plastic bottles. *Nature* **580**, 216–219 (2020).
14. Lu, H. *et al.* Machine learning-aided engineering of hydrolases for PET depolymerization. *Nature* **604**, 662–667 (2022).
15. Bååth, J. A., Borch, K., Jensen, K., Brask, J. & Westh, P. Comparative Biochemistry of Four Polyester (PET) Hydrolases. *ChemBioChem* **22**, 1627–1637 (2021).
16. Brizendine, R. K. *et al.* Particle Size Reduction of Poly(ethylene terephthalate) Increases the Rate of Enzymatic Depolymerization But Does Not Increase the Overall Conversion Extent. *ACS Sustain Chem Eng* **10**, 9131–9140 (2022).
17. Chow, J., Perez-Garcia, P., Dierkes, R. & Streit, W. R. Microbial enzymes will offer limited solutions to the global plastic pollution crisis. *Microb Biotechnol* **16**, 195–217 (2023).
18. Knott, B. C. *et al.* Characterization and engineering of a two-enzyme system for plastics depolymerization. *Proceedings of the National Academy of Sciences* **117**, 25476–25485 (2020).
19. Mrigwani, A., Thakur, B. & Guptasarma, P. Conversion of polyethylene terephthalate into pure terephthalic acid through synergy between a solid-degrading cutinase and a reaction

640 intermediate-hydrolysing carboxylesterase. *Green Chemistry* **24**, 6707–6719 (2022).
641 20. von Haugwitz, G. *et al.* Structural Insights into (Tere)phthalate-Ester Hydrolysis by a
642 Carboxylesterase and Its Role in Promoting PET Depolymerization. *ACS Catal* **12**, 15259–
643 15270 (2022).
644 21. Alves, V. D., Fontes, C. M. G. A. & Bule, P. Cellulosomes: Highly Efficient Cellulolytic
645 Complexes. *Subcell Biochem* **96**, 323–354 (2021).
646 22. Moraïs, S. *et al.* Cryptic diversity of cellulose-degrading gut bacteria in industrialized humans.
647 *Science* **383**, (2024).
648 23. Ramos, R., Domingues, L. & Gama, M. *Escherichia coli* expression and purification of LL37
649 fused to a family III carbohydrate-binding module from Clostridium thermocellum. *Protein*
650 *Expr Purif* **71**, 1–7 (2010).
651 24. Dueber, J. E. *et al.* Synthetic protein scaffolds provide modular control over metabolic flux.
652 *Nat Biotechnol* **27**, 753–759 (2009).
653 25. Makryniotis, K., Nikolaivits, E., Gkountela, C., Vouyiouka, S. & Topakas, E. Discovery of a
654 polyesterase from Deinococcus maricopensis and comparison to the benchmark LCCICCG
655 suggests high potential for semi-crystalline post-consumer PET degradation. *J Hazard Mater*
656 **455**, 131574 (2023).
657 26. Duarte, M. *et al.* Structure-function studies can improve binding affinity of cohesin-dockerin
658 interactions for multi-protein assemblies. *Int J Biol Macromol* **224**, 55–67 (2023).
659 27. Arnal, G. *et al.* Assessment of Four Engineered PET Degrading Enzymes Considering Large-
660 Scale Industrial Applications. *ACS Catal* **13**, 13156–13166 (2023).
661 28. Zhang, J. *et al.* Computational design of highly efficient thermostable MHET hydrolases and
662 dual enzyme system for PET recycling. *Commun Biol* **6**, 1135 (2023).
663 29. Wang, X., Lan, P. C. & Ma, S. Metal–Organic Frameworks for Enzyme Immobilization:
664 Beyond Host Matrix Materials. *ACS Cent Sci* **6**, 1497–1506 (2020).
665 30. Kucherenko, I. S., Soldatkin, O. O., Dzyadevych, S. V. & Soldatkin, A. P. Application of
666 zeolites and zeolitic imidazolate frameworks in the biosensor development. *Biomaterials*
667 *Advances* **143**, 213180 (2022).
668 31. Cai, X. *et al.* The Immobilization of Candida antarctica lipase B by ZIF-8 encapsulation and
669 macroporous resin adsorption: preparation and characterizations. *Biotechnol Lett* **42**, 269–
670 276 (2020).
671 32. Nakamura, M., Oyane, A., Inose, T., Kanemoto, Y. & Miyaji, H. One-Step Fabrication of
672 Water-Dispersible Calcium Phosphate Nanoparticles with Immobilized Lactoferrin for
673 Intraoral Disinfection. *Int J Mol Sci* **26**, 852 (2025).
674 33. Chen, K., Dong, X. & Sun, Y. Sequentially co-immobilized PET and MHET hydrolases via
675 Spy chemistry in calcium phosphate nanocrystals present high-performance PET degradation.
676 *J Hazard Mater* **438**, 129517 (2022).
677 34. Man, T. *et al.* Hierarchically encapsulating enzymes with multi-shelled metal-organic
678 frameworks for tandem biocatalytic reactions. *Nat Commun* **13**, 305 (2022).
679 35. Kim, H. T. *et al.* Biological Valorization of Poly(ethylene terephthalate) Monomers for
680 Upcycling Waste PET. *ACS Sustain Chem Eng* **7**, 19396–19406 (2019).
681 36. Weiland, F., Kohlstedt, M. & Wittmann, C. Biobased de novo synthesis, upcycling, and
682 recycling — the heartbeat toward a green and sustainable polyethylene terephthalate industry.
683 *Curr Opin Biotechnol* **86**, 103079 (2024).
684 37. Wongsatit, T., Srimora, T., Kiattisewee, C. & Uttamapinant, C. Enzymes, auxiliaries, and cells

for the recycling and upcycling of polyethylene terephthalate. *Curr Opin Syst Biol* **38**, 100515 (2024).

38. Pandit, A. V., Harrison, E. & Mahadevan, R. Engineering *Escherichia coli* for the utilization of ethylene glycol. *Microb Cell Fact* **20**, 22 (2021).

39. Valle-González, E. R., Jackman, J. A., Yoon, B. K., Mokrzecka, N. & Cho, N.-J. pH-Dependent Antibacterial Activity of Glycolic Acid: Implications for Anti-Acne Formulations. *Sci Rep* **10**, 7491 (2020).

40. Salusjärvi, L., Havukainen, S., Koivistoinen, O. & Toivari, M. Biotechnological production of glycolic acid and ethylene glycol: current state and perspectives. *Appl Microbiol Biotechnol* **103**, 2525–2535 (2019).

41. Reinbold, J. *et al.* Preventing Surgical Site Infections Using a Natural, Biodegradable, Antibacterial Coating on Surgical Sutures. *Molecules* **22**, 1570 (2017).

42. Montella, C. *et al.* Crystal Structure of an Iron-Dependent Group III Dehydrogenase That Interconverts L-Lactaldehyde and L-1,2-Propanediol in *Escherichia coli*. *J Bacteriol* **187**, 4957–4966 (2005).

43. Gao, H. *et al.* NADH oxidase from Lactobacillus reuteri: A versatile enzyme for oxidized cofactor regeneration. *Int J Biol Macromol* **123**, 629–636 (2019).

44. Chen, Z. *et al.* Biodegradation of highly crystallized poly(ethylene terephthalate) through cell surface codisplay of bacterial PETase and hydrophobin. *Nat Commun* **13**, 7138 (2022).

45. Chen, Z. *et al.* Enhanced in situ biodegradation of microplastics in sewage sludge using hyperthermophilic composting technology. *J Hazard Mater* **384**, 121271 (2020).

46. Gold, N. D. & Martin, V. J. J. Global View of the *Clostridium thermocellum* Cellulosome Revealed by Quantitative Proteomic Analysis. *J Bacteriol* **189**, 6787–6795 (2007).

47. Duarte, M. *et al.* A dual cohesin–dockerin complex binding mode in *Bacteroides cellulosolvens* contributes to the size and complexity of its cellulosome. *Journal of Biological Chemistry* **296**, 100552 (2021).

48. Ribitsch, D. *et al.* Fusion of Binding Domains to *Thermobifida cellulosilytica* Cutinase to Tune Sorption Characteristics and Enhancing PET Hydrolysis. *Biomacromolecules* **14**, 1769–1776 (2013).

49. Hwang, D.-H. *et al.* Enhanced biodegradation of waste poly(ethylene terephthalate) using a reinforced plastic degrading enzyme complex. *Science of The Total Environment* **842**, 156890 (2022).

50. Xu, T. *et al.* Small DNAs that Bind Nickel(II) Specifically and Tightly. *Anal Chem* **93**, 14912–14917 (2021).

51. Xu, C., Sun, L., Tong, S., Ouyang, J. & Gu, X. Cellulase immobilization on zeolitic imidazolate frameworks for boosting cellulose hydrolysis at high solids loading. *Ind Crops Prod* **206**, 117693 (2023).

52. Chen, K., Dong, X. & Sun, Y. Sequentially co-immobilized PET and MHET hydrolases via Spy chemistry in calcium phosphate nanocrystals present high-performance PET degradation. *J Hazard Mater* **438**, 129517 (2022).

53. Wang, L.-B. *et al.* A New Nanobiocatalytic System Based on Allosteric Effect with Dramatically Enhanced Enzymatic Performance. *J Am Chem Soc* **135**, 1272–1275 (2013).

54. Cui, Y. *et al.* Computational Redesign of a PETase for Plastic Biodegradation under Ambient Condition by the GRAPE Strategy. *ACS Catal* **11**, 1340–1350 (2021).

55. Zhong-Johnson, E. Z. L., Voigt, C. A. & Sinskey, A. J. An absorbance method for analysis of

enzymatic degradation kinetics of poly(ethylene terephthalate) films. *Sci Rep* **11**, 928 (2021).

56. Bell, E. L. *et al.* Directed evolution of an efficient and thermostable PET depolymerase. *Nat Catal* **5**, 673–681 (2022).

57. Liu, Y. *et al.* Enhancement of the degradation capacity of IsPETase for PET plastic degradation by protein engineering. *Science of The Total Environment* **834**, 154947 (2022).

58. Liu, Z., Zhang, Y. & Wu, J. Enhancement of PET biodegradation by anchor peptide-cutinase fusion protein. *Enzyme Microb Technol* **156**, 110004 (2022).

59. Hayes, H. C. & Luk, L. Y. P. Investigating the effects of cyclic topology on the performance of a plastic degrading enzyme for polyethylene terephthalate degradation. *Sci Rep* **13**, 1267 (2023).

60. Cui, Y. *et al.* Computational redesign of a hydrolase for nearly complete PET depolymerization at industrially relevant high-solids loading. *Nat Commun* **15**, 1417 (2024).

61. Carniel, A., Valoni, É., Nicomedes, J., Gomes, A. da C. & Castro, A. M. de. Lipase from *Candida antarctica* (CALB) and cutinase from *Humicola insolens* act synergistically for PET hydrolysis to terephthalic acid. *Process Biochemistry* **59**, 84–90 (2017).

62. de Castro, A. M., Carniel, A., Nicomedes Junior, J., da Conceição Gomes, A. & Valoni, É. Screening of commercial enzymes for poly(ethylene terephthalate) (PET) hydrolysis and synergy studies on different substrate sources. *J Ind Microbiol Biotechnol* **44**, 835–844 (2017).

63. Barth, M. *et al.* A dual enzyme system composed of a polyester hydrolase and a carboxylesterase enhances the biocatalytic degradation of polyethylene terephthalate films. *Biotechnol J* **11**, 1082–1087 (2016).

64. Gao, J. *et al.* Degradation Kinetic Studies of BSA@ZIF-8 Nanoparticles with Various Zinc Precursors, Metal-to-Ligand Ratios, and pH Conditions. *ACS Omega* **8**, 44601–44610 (2023).

65. Duan, X. *et al.* ZIF-8 as a protein delivery system enhances the application of dental pulp stem cell lysate in anti-photoaging therapy. *Mater Today Adv* **17**, 100336 (2023).

Author information

Authors and Affiliations

College of Life Sciences, Northwest A&F University, Yangling, Shaanxi, China

Yujia Zhang, Chongsen Li, Yanbing Lin

Institute of Molecular Physiology, Shenzhen Bay Laboratory, Shenzhen, China

Yujia Zhang, Chongsen Li, Ehsan Hashimi, Hui Gao, Zhuobin Liang

School of Science, Harbin Institute of Technology (Shenzhen), Shenzhen, China

Enting Xu, Xuemei Yang

Contributions

Yujia Zhang: Methodology, Investigation, Data Curation, Formal Analysis, Visualization, Writing – Original Draft. **Chongsen Li:** Investigation, Data Curation, Validation. **Ehsan Hashimi**: Investigation, Data Curation, Validation. **Enting Xu:** Investigation, Validation. **Xuemei Yang:** Methodology, Supervision, **Yanbing Lin:** Resources, Supervision. **Hui Gao:** Conceptualization, Methodology, Investigation, Data Curation, Formal Analysis, Writing – Original Draft, Funding acquisition. **Zhuobin Liang:** Conceptualization, Methodology, Supervision, Writing – Original Draft, Project administration, Funding acquisition.

Corresponding authors

Correspondence to Zhuobin Liang or Hui Gao.

Extended Data

Source Data

Supplementary information

Supplementary Tables 1-4

Supplementary Figure 1-16

Supplementary File 1

Supplementary Methods

782 **Supplementary Table 1. Key degradation parameters and efficiency of major PET hydrolases**

PET hydrolase	PET substrate*	Reaction condition	Enzyme usage (nmol)	Total products (mM)	Degradation efficiency (mol total products /mmol enzyme)	Reference
IsPETase	Film-L	30 °C, 18 h, pH 7.0	0.015	0.30	6.00	12
TfH			0.015	0.00079	0.016	
LCC			0.015	0.0063	0.13	
FsC			0.015	0.00075	0.015	
LCC	Post-consumer colored-flake PET waste-H	72 °C, 20 h, pH 8.0	690.00	552.09	64.01	13
ICCG ($LCC^{F243I/D238C/S283C/Y127G}$)		72 °C, 15 h, pH 8.0	690.00	854.17	99.03	
WCCG ($LCC^{F243W/D238C/S283C/Y127G}$)		72 °C, 20 h, pH 8.0	690.00	885.42	102.66	
FAST-PETase ($IsPETase^{S121E/D186H/R224Q/N233K/R280A}$)	Film-H	50 °C, 96 h, pH 8.0	0.12	33.80	169.00	14
ICCM ($LCC^{F243I/D238C/S283C/N246M}$)			0.12	29.50	147.50	
		40 °C, 96 h, pH 8.0	0.12	14.75	73.75	
DuraPETase ($IsPETase^{S214H/I168R/W159H/S188Q/R280A/A180I/G165A/Q119Y/L117F/T140D}$)	Film-H	50 °C, 72 h, pH 9.0	0.17	2.63	7.56	54
		37 °C, 72 h, pH 9.0	0.17	1.76	5.06	
LCC			0.17	1.04	3.00	
TS-PETase ($IsPETase^{S121E/D186H/R280A}$)	Film-L	30 °C, 6 days, pH 9.0	0.40	0.05	0.13	55
fvThermobifida fusca $cutinase^{H184S/Q92G/F209I/I213K}$	Bottle-H	60 °C, 96 h, pH 8.0	1461.18	N/A (3542.00 nmol)	2.42	44
$LCC^{H184S/Q92G/F209I/I213K}$			1742.22	N/A (1354.00 nmol)	0.78	
$BhrPETase^{H184S/Q92G/F209I/I213K}$			1724.14	N/A (3802.00 nmol)	2.21	
HotPETase	Powder-H	60 °C, 5 h, pH 9.2	0.21	6.07	146.52	56
DuraPETase-4M ($DuraPETase^{N233C/S282C/H214S/S245R}$)	Powder-H	60 °C, 96 h, pH 9.0	0.01	15.80	45.48	57
DuraPETase			0.01	5.70	16.39	
DSI- $Tfcutinase^{D204C/E253C}$ (Tfuc2 fusing with the anchor peptide Dermaseptin SI)	Particle-L	70 °C, 96 h, pH 8.0	7.00	300.00	42.86	58
IsPETase-Spy (Cyclic monomer)	Powder-H	30 °C, 24 h, pH 7.5	0.10	0.40	4.03	59
IsPETase-Dimer (Cyclic dimer)			0.05	0.46	9.16	
IsPETase-Cat (Catenane)			0.05	0.50	9.95	
IsPETase			0.10	0.40	3.95	
TurboPETase	Film-L	65 °C, 12 h, pH 8.0	0.16	130.00	401.04	60
BhrPETase			0.16	6.00	18.54	
LCC^{ICCG}			0.16	34.00	104.41	
FAST-PETase			0.15	2.00	6.89	

783 Note: **a** * Substrates can vary in different studies. To facilitate their comparison, we define substrates as follows L:
784 low crystallinity (< 20%), H: high crystallinity (> 20%). **b** Total products include TPA, MHET, and BHET. 3. Extended
785 details associated of this table is provided in **Supplementary File 1**. **c** N/A: information not available from the
786 corresponding publication.

787 **Supplementary Table 2. Current multi-enzyme systems for biodegradation of PET plastics**

System	PET substrate*	Reaction condition	Enzymes	Total products (mM)	Reaction volume (mL)	Degradation efficiency (mol total products /mmol enzyme)	Reference condition in this study	Reference
HiC+CALB	Bottle-H	60 °C, 14 days, pH 7	225 nmol HiC + 24.24 nmol CALB	2.247	5	0.045	★	61
HiC+CALB	Bottle-H	60 °C, 14 days, pH 7	62.5 nmol HiC + 60.61 nmol CALB	0.728	10	0.06	★	62
TfCa+LCC	Film-L	60 °C, 24 h, pH 9	21.7 nmol TfCa (immobilized) + 13.85 nmol LCC	10.42 (TPA: 6.71, M/BHET: 3.71)	40	11.72	♠	63
PETase+ MHETase	Film-L	30 °C, 96 h, pH 7.5	0.33 nmol PETase + 0.081 nmol MHETase	2.87	0.5	3.47	♣	18
cPETase+ cCALB+ mCbpA (scaffold)	Waste-H	30 °C, 96 h pH 7	10 nmol cPETase + 10 nmol cCALB	0.04	40+	0.08	♦	49
	Film-H			0.089		0.18	♦	
LCC+TTCE	Film-L	60 °C, 96 h, pH 8	1 nmol LCC + 1 nmol TTCE	17.97	0.5	4.49	♣	19
TfCaWA+ IsPETasePM	Film-L	45 °C, 24 h, pH 7.5	0.05 nmol PETase + 0.55 nmol TfCa	1.68	1	2.80	♠	20
SPEED (FAST-PETase+ MHETase+ ICCG+Scaffold.4)	(♠) Film-L	40 °C, 24 h, pH 7	0.25 nmol FAST + 0.25 nmol MHETase + 0.25 nmol ICCG	82.87	0.5	55.25	-	This study **Fig. 4f** (1-day)
	(♥) Powder-H	40 °C, 96 h, pH 7		143.76		95.84	-	**Fig. 4e** (4-day)
	(♣) Film-L			148.82		99.21	-	**Fig. 4f** (4-day)
	(♦) Film-H			3.23		2.15	-	**Fig. 4g** (4-day)
	(■) Film-L	40 °C, 14 days, pH 7		189.85		126.57	-	**Fig. 4f** (14-day)
	(★) Film-H			9.05		6.03	-	**Fig. 4g** (14-day)

788 Note: **a** * Substrates can vary in different studies. To facilitate their comparison, we define substrates as follows: L:
789 low crystallinity (< 20%), H: high crystallinity (> 20%). **b** + Where reaction volume was not specified in the original
790 publication nor provided by the corresponding author, a reaction volume of 40 mL was assumed for efficiency
791 calculations, based on the largest volume reported in similar studies listed in this table. **c** Total products include TPA,
792 MHET, and BHET. **d** Symbols (♠, ♥, ♣, ♦, ■, ★) denote analogous reaction conditions from this study, provided for
793 contextual reference. **e** Extended details associated of this table is provided in **Supplementary File 1**.

794 **Supplementary Table 3. Copy number of enzyme and scaffold expression cassettes in the genome**
795 **of the engineered *P. pastoris* strains**

Strain	Expression cassette	Copy number
SMD1168$_{His4::CipA\text{-}CBM\text{-}CipC\text{-}SED1}$	CipA-CBM-CipC-SED1	22.13±1.14
SMD1168$_{His4::MHETase}$	MHETase	17.71±0.99
SMD1168$_{His4::FAST}$	FAST	15.20±0.38
SMD1168$_{His4::FAST\text{-}MHETase}$	MHETase	18.19±0.72
SMD1168$_{His4::FAST\text{-}MHETase}$	FAST	14.54±0.77

796

797 **Supplementary Table 4. Calculated PET conversion extents for key reactions in this study**

Reaction	Released TPA (mM)	Released MHET (mM)	Released BHET (mM)	Conversion extent (% of total substrate)	Reaction condition	Data source
Complex-B +PET powder	19.49	2.62	0.00	2.50%	30 °C, pH 7.0, 4 days	Fig.1f, the last bar
Complex-B +PET Film-L	17.29	0.00	0.00	1.97%	30 °C, pH 7.0, 4 days	Fig.1g, the last bar
Complex-B +PET Film-H	0.71	0.01	0.01	0.08%	30 °C, pH 7.0, 4 days	Fig.1h, the last bar
Complex-C +PET powder	22.37	1.63	0.20	2.75%	30 °C, pH 7.0, 4 days	Fig.2f, the last bar
Complex-C +PET Film-L	23.22	0.00	0.27	2.68%	30 °C, pH 7.0, 4 days	Fig.2g, the last bar
optiComplex-D +PET powder	145.95	43.36	0.79	21.29%	70 °C, pH 7.0, 4 days	Fig.4c, the last bar
optiComplex-D +PET powder	140.30	1.42	2.04	16.40%	40 °C, pH 7.0, 4 days	Fig.4e, 4-day
optiComplex-D +PET powder	170.18	1.92	2.14	19.87%	40 °C, pH 7.0, 17 days	Fig.4e, 17-day
optiComplex-D +PET Film-L	146.75	0.43	1.65	16.98%	40 °C, pH 7.0, 4 days	Fig.4f, 4-day
optiComplex-D +PET Film-L	201.89	0.00	0.00	23.02%	40 °C, pH 7.0, 17 days	Fig.4f, 17day
optiComplex-D @ZIF-8(i) +PET powder	215.73	3.74	0.00	24.99%	40 °C, pH 7.0, 4 days	Fig.5c, 4 days' point
optiComplex-D @ZIF-8(i) +PET powder	293.38	0.47	0.00	33.49%	40 °C, pH 7.0, 14 days	Fig.5c, 14-day
optiComplex-D @ZIF-8(ii) +PET powder	237.19	0.63	0.23	27.14%	40 °C, pH 7.0, 4 days	Fig.5c, 4-day
optiComplex-D @ZIF-8(ii) +PET powder	276.94	1.65	0.00	31.74%	40 °C, pH 7.0, 14 days	Fig.5c, 14-day
optiComplex-D @CaP +PET Film-L	255.09	0.00	0.00	29.08%	40 °C, pH 7.0, 4 days	Fig.S15b, 4-day
optiComplex-D @CaP +PET Film-L	319.84	2.44	0.00	36.72%	40 °C, pH 7.0, 14 days	Fig.S15b, 14-day
optiComplex-D +Complex-E +PET powder	197.14	0.00	0.00	22.47%	40 °C, pH 7.0, 4 days	Fig.6e, the last bar

798 Note: PET conversion extent (%) was calculated from the total moles of released products (TPA, MHET, and BHET),
799 as quantified by HPLC, relative to the initial molar quantity of PET repeating units (details in **Supplementary**
800 **Methods**). The crystallinity of the substrates was determined to be 40.82% (PET powder), 17.99% (Film-L).
801

Supplementary Table 5. Information of key genes and primers of this study

Type	Gene	Sequence
Enzyme	FAST-PETase-CelK	catatgcagacaaatccctatgcccgtgggccaaatcccactgcggcgagtttagaagccagtgccggtccgtttaccgtccgttctttttactgtaagccgcccgtccggatacgg ggcgggggacggtttattatcccacgaatgccggaggcaccgtgggtgctattgcaattgttccaggctatacagcgcgccaatcatctatcaaatggtggggaccgcgtctggct tcgcacggattcgtagttattacgattgacacaaacagcacgttagaccagcccgaaagtcgcagcagtcaacaaatggcggcgttacgtcaggtcgcaagcttaaacgggaca tcaagcagtcccatctatggaaaagtcgatacagcgcgcatgggtgtcatgggctggtccatgggaggcgggggtctttgatttctgctgctaataatcctagtttaaaagccgc cgccccgcaggcaccgtggcattcgtccaccaacttttcatcggtaacggtccccactcttatttttgcgtgtgagaacgactcgatcgcaccggttaattcttctgctctgccgattt acgactcaatgtcgcaaaatgcaaagcaattccttgaaattaaaggtggctcccattcttgtgccaactcaggtaacagtaatcaagcccttattggaaagaaaggtgtcgcatgga tgaaacgttttatggataatgacacccgctattctaccttcgcctgcgaaaacccgaacagcaccgctgtatcagatttccgcactgccaactgtagcttaataacaccgccaggag gagtagacccagaagaaccggaggttatttatggtgactgcaatggcgacggaaaagttaattcaactgacgctgtggcattgaagagatatatcttgagatcaggtataagcatc aacactgataatgctgatgtaaatgctgatggcagagttaactctacagacttggcaatattgaagagatatattcttaaagagatagatgtattgccacataaactcgag
Enzyme	MHETase-linker-CelF	catatgcagaccacagtaacgacgatgttgcttgcaagcgtagccttagccgcctgtgcgggtggtggcagcaccccattaccgttaccgcaacaacagccgccccagcaaga accacccccaccgcctgtcccgttagcgtcacgcgcagcatgtgaggcactgaaagacggcaatggcgacatggtatggccgaatgccgctaccgtggtcgaagtcgctgcc tggcgcgacgcggcaccagctacagcaagtgctgctgcactgcctgaacactgcgaagtgtcgggcgcgatcgcgaaacgcacgggcattgatggctacccgtacgaaatta aatttcgtcttcgtatgccagcggaatggaatggacgtttcttcatggagggcggctcggggacaaatggttcattgtcagcggctacaggttcgattgggggtggtcaaattgcat ctgccttgagccgcaacttcgccaccatcgctaccgacggagggcatgataacgcggttaatgacaacccggatgcattgggaacagttgcctttggtttagatccccaggctcg tctggacatgggctacaataggttacgaccaggtcacgcaagctggcaaggctgcggttgctcgtttctatggacgtgcggcagacaaatcgtatttcattggatgcagtgaggga ggacgcgagggcatgatgctgagccagcgctttccatcacactacgatggcattgtcgccggtgcccctgggtatcagctgccaaaagccgggatttccggtgcctggacgac gcaatccttggcaccagccgcagtcgggttagatgcgcaaggggtgcctctgattaataagtccttctcggatgctgatttgcaccttctgtcacaagctatcttaggaacatgtgac gctctggatggattggcagatggaattgttgacaactaccgcgcctgtcaggcagcgttcgatcccgctacagctgcgaatccggctaacggtcaggccttgcaatgtgtcggg gcaaagacagcagactgcctgtctcctgtgcaggtgaccgctatcaaacgcgcgatggcagggccagtgaattctgcaggcaccccccctgtataatcgttgggcgtgggacgc tggtatgagtggcttgtcagggacaacgtataatcagggatggcgcagctggtggttggggtctttcaacagctctgcgaataacgcgcaaaaggtcagcggcttcgcggctcg ttcctggctggtggatatcgcaactcccaccagagcccatgcctatgacccaggttgctgcacgcatgatgaaattcgacttcgatattgatccgctgaaaatttgggcgacatctgg gcaatttacacaaagctctatggactggcacggcgctacttcgaccgatttagcggcttttcgtgaccgtggaggcaagatgatcttgtatcacggtatgagtgatgcggccttcag tgcattagatacggcggattattacgagcgtctgggagcggctatgcctggggctgccggtttcgctcgccttttttagtaccagggatgaaccattgctcaggcgggcctggaa cggaccgttttgacatgttgactcctttagtggcctgggttgagcgtggcgaggcgcctgatcaaatttccgcatggtccgggaccccagggtatttcggtgttgcagcacgcacc cgcccgttgtgtccatatccacaaatcgcgcgttataaagggtccggagacattaatacggaagcgaattttgcttgcgcagcccccccctcccagatcaaggtccagaaaaatt attgggtgatgtaaacggtgacgaaactgtagacgctattgaccttgctatacttaaaaatatcttttaaacagcagtactacaataaatactgcaaatgcagatatgaatagtgata atgctattgacgctattgactatgctcttttaaagaaagcacttctttctatccaactcgag
Enzyme	optiMHETase--linker-CelF	ggtggtggtagtacaccgctgccgctgcctcagcagcagcctccgcagcaagaaccgcctccgcctccggttccgctggcaagccgtgcagcatgtgaagcactgaaagatg gtaatggtgatatggtttggccgaatgcagcaaccgttgttgaagttgcagcatggcgtgatgcagcaccggcaaccgcaagcgcagcagcactgccggaacattgtgaagtta gcggtgcaattgccaaacgtaccggtattgatggttatccgtatgaaatcaaatttcgtctgcgtatgcctgcagaatggaatggtcgtttctttatggaaggtggtagcggcaccaa tggtagcctgagcgcagcaccggtagcattggtggtggtcagattgcaagcgcactgagccgtaattttgcaaccattgcaaccgatggtggtcatgataatgccgttaatgata atccggatgcactgggcaccgttgcatttggtctggatccgcaggcacgtctggatatgggttataatagctatgatcaggttacccaggcaggtaaagcagcagttgcacgttttt atggtcgtgcagcagataaaagctattttatcggttgtagcgaaggtggtcgtgaaggtatgatgctgagccagcgttttccgagccattatgatggtattgttgcgggtgcaccgg gttatcagctgccgaaagcaggtattagtggtgcatggaccacacagagcctggcaccggcagccgttggcctggatgcacagggtgttccgctgattaacaaaagctttagtg atgccgatctgcatctgctgagtcaggcaattctgggcacctgtgatgccctggatggtctggcagatggcattgttgataactatcgtgcatgtcaggcagcatttgatccggcaa cagcagcaaatccggcaaatggtcaggccctgcagtgtgttggtgcaaaaaccgcagattgtctgagtccggttcaggtgaccgcaattaaacgcgcaatggcaggtccggtta atagcgcaggcacaccgctgtataatcgttgggcatgggatgcaggtatgagcggtctgagcggtacaacctataatcaaggttggcgtagttggtggctgggtagctttaatag cagcgcaaataatgcccagcgtgttagcggttttagcgcacgtagctggctggttgattttgcgacccctccggaaccgatgccgatgacacaggttgcagcacgcatgatgaaa ttcgattttgatattgacccgctgaaaatttgggcaaccagcggtcagtttacccagagtagcatggattggcatggtgcaaccagcaccgatctggcagcctttcgtgatcgtggt ggtaaaatgattctgtatcatggtatgtcagatgcagcctttagtgcactggatacagcagattattatgaacgtctgggtgcagcaatgcctggtgcagcaggttttgcacgtctgtt tctggttccgggtatgaatcattgtagcggtggtccgggtacagatcgttttgatatgctgacccctctggttgcatgggttgaacgtggtgaagcaccggatcagattagcgcatg gtcaggtactccgggttattttggtgttgccgcacgtacccgtccgctgtgtccgtatccgcagatcgcacgttataaaggtagcggtgatattaacaccgaagccaattttgcatgt gcagcacctccgttcccagatcaaggtccagaaaaattattggtgatgtaaacggtgacgaaactgtagacgctattgaccttgctatacttaaaaaatatctttttaaacagcagta ctacaataaatactgcaaatgcagatatgaatagtgataatgctattgacgctattgactatgctcttttaaagaaagcacttctttctatccaa
Enzyme	$SH3_L$-linker-optiMHETase	cctcctcctgctctgccaccaaaaaggagaagatctggaggtggaggctcaggaggtggaggctccggaggtggaggctcaggtggtggtagtacaccgctgccgctgcctc agcagcagcctccgcagcaagaaccgcctccgcctccggttccgctggcaagccgtgcagcatgtgaagcactgaaagatggtaatggtgatatggtttggccgaatgcagca accgttgttgaagttgcagcatggcgtgatgcagcaccggcaaccgcaagcgcagcagcactgccggaacattgtgaagttagcggtgcaattgccaaacgtaccggtattgat ggttatccgtatgaaatcaaatttcgtctgcgtatgcctgcagaatggaatggtcgtttctttatggaaggtggtagcggcaccaatggtagcctgagcgcagccaccggtagcatt ggtggtggtcagattgcaagcgcactgagccgtaattttgcaaccattgcaaccgatggtggtcatgataatgccgttaatgataatccggatgcactgggcaccgttgcatttggt ctggatccgcaggcacgtctggatatgggttataatagctatgatcaggttacccaggcaggtaaagcagcagttgcacgtttttatggtcgtgcagcagataaaagctattttatcg gttgtagcgaaggtggtcgtgaaggtatgatgctgagccagcgttttccgagccattatgatggtattgttgcgggtgcaccgggttatcagctgccgaaagcaggtattagtggt gcatggaccacacagagcctggcaccggcagccgttggcctggatgcacagggtgttccgctgattaacaaaagctttagtgatgccgatctgcatctgctgagtcaggcaattc tgggcacctgtgatgccctggatggtctggcagatggcattgttgataactatcgtgcatgtcaggcagcatttgatccggcaacagcagcaaatccggcaaatggtcaggccct gcagtgtgttggtgcaaaaaccgcagattgtctgagtccggttcaggtgaccgcaattaaacgcgcaatggcaggtccggttaatagcgcaggcacaccgctgtataatcgttgg gcatgggatgcaggtatgagcggtctgagcggtacaacctataatcaaggttggcgtagttggtggctgggtagctttaatagcagcgcaaataatgcccagcgtgttagcggttt tagcgcacgtagctggctggttgattttgcgacccctccggaaccgatgccgatgacacaggttgcagcacgcatgatgaaattcgattttgatattgacccgctgaaaatttgggc aaccagcggtcagtttacccagagtagcatggattggcatggtgcaaccagcaccgatctggcagcctttcgtgatcgtggtggtaaaatgattctgtatcatggtatgtcagatgc agcctttagtgcactggatacagcagattattatgaacgtctgggtgcagcaatgcctggtgcagcaggttttgcacgtctgtttctggttccgggtatgaatcattgtagcggtggtc cgggtacagatcgttttgatatgctgacccctctggttgcatgggttgaacgtggtgaagcaccggatcagattagcgcatggtcaggtactccgggttattttggtgttgccgcac gtacccgtccgctgtgtccgtatccgcagatcgcacgttataaaggtagcggtgatattaacaccgaagccaattttgcatgtgcagcacctccg
Enzyme	OptiMHETase--linker-$SH3_L$	ggtggtggtagtacaccgctgccgctgcctcagcagcagcctccgcagcaagaaccgcctccgcctccggttccgctggcaagccgtgcagcatgtgaagcactgaaagatg gtaatggtgatatggtttggccgaatgcagcaaccgttgttgaagttgcagcatggcgtgatgcagcaccggcaaccgcaagcgcagcagcactgccggaacattgtgaagtta gcggtgcaattgccaaacgtaccggtattgatggttatccgtatgaaatcaaatttcgtctgcgtatgcctgcagaatggaatggtcgtttctttatggaaggtggtagcggcaccaa tggtagcctgagcgcagccaccggtagcattggtggtggtcagattgcaagcgcactgagccgtaattttgcaaccattgcaaccgatggtggtcatgataatgccgttaatgata atccggatgcactgggcaccgttgcatttggtctggatccgcaggcacgtctggatatgggttataatagctatgatcaggttacccaggcaggtaaagcagcagttgcacgttttt atggtcgtgcagcagataaaagctattttatcggttgtagcgaaggtggtcgtgaaggtatgatgctgagccagcgttttccgagccattatgatggtattgttgcgggtgcaccgg gttatcagctgccgaaagcaggtattagtggtgcatggaccacacagagcctggcaccggcagccgttggcctggatgcacagggtgttccgctgattaacaaaagctttagtg atgccgatctgcatctgctgagtcaggcaattctgggcacctgtgatgccctggatggtctggcagatggcattgttgataactatcgtgcatgtcaggcagcatttgatccggcaa cagcagcaaatccggcaaatggtcaggccctgcagtgtgttggtgcaaaaaccgcagattgtctgagtccggttcaggtgaccgcaattaaacgcgcaatggcaggtccggtta atagcgcaggcacaccgctgtataatcgttgggcatgggatgcaggtatgagcggtctgagcggtacaacctataatcaaggttggcgtagttggtggctgggtagctttaatag cagcgcaaataatgcccagcgtgttagcggttttagcgcacgtagctggctggttgattttgcgacccctccggaaccgatgccgatgacacaggttgcagcacgcatgatgaaa ttcgattttgatattgacccgctgaaaatttgggcaaccagcggtcagtttacccagagtagcatggattggcatggtgcaaccagcaccgatctggcagcctttcgtgatcgtggt ggtaaaatgattctgtatcatggtatgtcagatgcagcctttagtgcactggatacagcagattattatgaacgtctgggtgcagcaatgcctggtgcagcaggttttgcacgtctgtt tctggttccgggtatgaatcattgtagcggtggtccgggtacagatcgttttgatatgctgacccctctggttgcatgggttgaacgtggtgaagcaccggatcagattagcgcatg gtcaggtactccgggttattttggtgttgccgcacgtacccgtccgctgtgtccgtatccgcagatcgcacgttataaaggtagcggtgatattaacaccgaagccaattttgcatgt gcagcacctccgtctggaggtggaggctcaggaggtggaggctccggaggtggaggctcacctcctcctgctctgccaccaaaaaggagaagatga
Enzyme	ICCG-ScaA	agcaacccgtaccagcgtggcccgaatccgacccgcagcgcactgaccgcagatggcccgtttagcgtggcaacctacaccgtctcacgcctgtcagtctcgggttttggcgg tggcgtgatttattacccgaccggcacgtctctgacgttcggtggcatcgcgatgagtcccgggttatacccgcagatgctagctctctggcatggctgggtcgtcgcctggcttccc atggctttgtggttctggtgattaacacgaattcacgtttcgatggcccggacagccgcgcctctcagctgagtgccgccctgaactacctgcgtaccagttccccgagcgccgtt cgcgcacgtctggatgcaaatcgtctggcggttgccggtcattctatgggtggcggtggcaccctgcgtattgcagaacaaaacccgagcctgaaagcggctgtcccgctgac cccgtggcacaccgataaaacgtttaataccagtgtcccggtgctgattgttggcgcagaagctgacaccgtggcgccggtttcgcagcatgccatcccgttttatcaaaacctgc cgagcaccacgccgaaagtttacgtcgaactgtgcaacgcatcgcacattgctccgaacagcaacaatgcggccatttccgtttatacgatctcatggatgaaactgtgggtcgat

		aatgacacccgttaccgccagttcctgtgtaatgtgaacgacccggctctgtgcgacttccgcaccaataatcgccactgccaagtaacaactcctcagcccggcacaaagctcg ttcctacatggggcgatacaaactgcgacggcgttgtaaatgttgctgacgtagtagttcttaacagattcctcaacgatcctacatattctaacattactgatcagggtaaggttaac gcagacgttgttgatcctcaggataagtccggcgcagcagttgatcctgcaggcgtaaagctcacagtagctgactctgaggcaatcctcaaggctatcgttgaa
Enzyme	FucO-linker-CelF	atgatggctaacagaatgctggtgaacgaaacggcatggtttggtcgaggtgctgttggagctttaaccgatgaagtgaaacgccgtggttatcagaaggcgctgatcgtcaccg ataaaacgctggtgcaatgcggcgtggtggcgaaagtgaccgacaagatggatgccgcaggactggcatgggcgatttacgacggcgtagtacctaacccaacaattactgtc gtcaaagaagggctcgatgtattccagaatagcggcgcggattacctgatcgctattggtggtggttctccacaggatacgtgtaaagcgattggcattatcagcaacaacccgg agtttgccgatgtgcgtagcctggaagggctttccccgaccaataaacccagtgtaccgattctggcaatccccaccacgcaggcactgcggcagaagtgaccattaactacg tgatcactgacgaagagaaacggcgcaagtttgtttgcgttgatccgcatgatatcccgcaggtggcgtttattgacgctgacatgatggatggtatgcctccagcgctgaaagct gcgacgggtgtcgatgcgctcactcatgctattgaggggtatattacccgtggcgcgtgggcgctaaccgatgcactgcacattaaagcgattgaaatcattgctggggcgctgc gaggatcggttgctggtgataaggatgccggagaagaaatggcgctcgggcagtatgttgcgggtatgggcttctcgaatgttgggttagggttggtgcatggtatggcgcatcc actgggcgcgttttataacactccacacggtgttgcgaacgccatcctgttaccgcatgtcatgcgttataacgctgactttaccggtgagaagtaccgcgatatcgcgcgcgttat gggcgtgaaagtggaaggtatgagcctggaagaggcgcgtaatgccgccgttgaagcggtgtttgctctcaaccgtgatgtcggtattccgccacatttacgtgatgttggtgtac gcaaggaagacattccggcactggcgcaggcggcactggatgatgtttgtaccggtggcaacccgcgtgaagcaacgcttgaggatattgtagagctttaccataccgcctggt ctggaggtggaggctcaggaggtggaggctctggaggtggaggctcaggaggtggaggctcacctaggttcccagatcaaggtccagaaaaattattgggtgatgtaaacgg tgacgaaactgtagacgctattgaccttgctatacttaaaaaatatcttttaaacagcagtactacaataaatactgcaaatgcagatatgaatagtgataatgctattgacgctattga ctatgctcttttaaagaaagcacttctttctatccaactcgag
Enzyme	$SH3_L$-linker-AldA	cctcctcctgctctgccaccaaaaaggagaagatctggaggtggaggctcaggaggtggaggctcccggaggtggaggctcacatatgtcagtacccgttcaacatcctatgtat atcgatggacagtttgttacctggcgtggagacgcatggattgatgtggtaaaccctgctacagaggctgtcatttcccgcatacccgatggtcaggccgaggatgcccgtaagg caatcgatgcagcagaacgtgcacaaccagaatgggaagcgttgcctgctattgaacgcgccagttggttgcgcaaaatctccgccgggatccgcgaacgcgccagtgaaat cagtgcgctgattgttgaagaagggggcaagatccagcagctggctgaagtcgaagtggcttttactgccgactatatcgattacatggcggagtgggcacggcgttacgaggg cgagattattcaaagcgatcgtccaggagaaaatattcttttgtttaaacgtgcgcttggtgtgactaccggcattctgccgtggaacttcccgttcttcctcattgcccgcaaaatgg ctcccgctcttttgaccggtaataccatcgtcattaaacctagtgaatttacgccaaacaatgcgattgcattcgccaaaatcgtcgatgaaataggccttccgcgcggcgtgtttaa ccttgtactggggcgtggtgaaaccgttgggcaagaactggcgggtaacccaaggtcgcaatggtcagtatgacaggcagcgtctctgcaggtgagaagatcatggcgactg cggcgaaaaacatcaccaaagtgtgtctggaattgggggggtaaagcaccagctatcgtaatggacgatgccgatcttgaactggcagtcaaagccatcgttgattcacgcgtcat taatagtgggcaagtgtgtaactgtgcagaacgtgtttatgtacagaaaggcatttatgatcagttcgtcaatcggctgggtgaagcgatgcaggcggttcaatttggtaaccccgc tgaacgcaacgacattgcgatggggccgttgattaacgccgcggcgctggaaagggtcgagcaaaaagtggcgcgcgcagtagaagaaggggcgagagtggcgttcggtg gcaaagcggtagaggggaaaggatattattatccgccgacattgctgctggatgttcgccaggaaatgtcgattatgcatgaggaaacctttggcccggtgctgccagttgtcgc atttgacacgctggaagatgctatctcaatggctaatgacagtgattacggcctgacctcatcaatctataccccaaaatctgaacgtcgcgatgaaagccattaaagggctgaagtt ggtgaaacttacatcaaccgtgaaaacttcgaagctatgcaaggcttccacgccggatggcgtaaatccggtattggcggcgcagatggtaaacatggcttgcatgaatatctgc agacccaggtggtttatttacagtcgctcgag
Enzyme	LrNox-linker- ScaA	atgaaggttattattgttggttgtacacatgcgggaacaattactgccactcaaattttacagaatcatccagaaacagaagtcacaatttatgaacggaatgataacgtttcattcctct catgtgggattgcagtttactgagcggtgatgttggtaatccagatgcgatgttttatcaagccctgaacaacttgctgccatgggtgcaacagttcatatgcaacaatatgtaact gatattgaccctaagactaagacagtcacagtgacagaccttgtgacaggcgaaacaaagaccgaccattatgataagttagttgatactactggttcttggccagtaattccacca attgaaggtgtagatggccctcatgtttatttgtgcaagaattaccatcatgctaaagaattatttaacgttgctaaagatgcgcaacgaattgttgtgattggtggaggttatattgggg ttgaattagtagaagcttacactcgtcaaaataaggacgttacattgattgatgggtctccacggatgcttcataaatactttgaccgcgagtatacggatcgaattcaacaggaattt gtagatcacggcgcccactttgcttttgaccaacgcgtaactggatttgaaaaccacgaaaatggtgtaaccgttaagacggataaggggcaactacgaggcagatattgctatcct ctgtgttggcttccgtcctaatactgatctcttaaaaggtaaagttaagatgcatgataatggggcaatcattacgaacgaatacatgcaatcatctgatccagatatttacgctgccg gagattcaacggctgttcactataacccaactggcaaggatgcatacattccattagctactaacgctattcggcaaggaacaattgttggaacaaatctctttggtaatacaatgcg cgatatgggaacccaatctagttctggcttaaacttatatggaacaacgatggtatcatctggcttaactttggagaatgccaaagaagcgggctttgatgcagctgcggtgacagt tgaagacaactaccgtccagaatttatgccgacaacaactcctgtattaatgacattggtgtgggataagaagactcggcaaattcttggtggacagtttatgagtaagcatgatgttt ctcaatctgctaacattatttccttatgtatccaggataagcacacgattgattatttagcatttgttgatatgcttttccaaccacactttgatcgtccatttaactatgtaaatattcttggcc aagcggcggtaaagaaacaagctgaattagaaaaatctggaggtggaggctcaggaggtggaggctccggaggtggaggctcacctagggtaacaactcctcagcccggc acaaagctcgttcctacatggggcgatacaaactgcgacggcgttgtaaatgttgctgacgtagtagttcttaacagattcctcaacgatcctacatattctaacattactgatcagggg taaggttaacgcagacgttgttgatcctcaggataagtccggcgcagcagttgatcctgcaggcgtaaagctcacagtagctgactctgaggcaatcctcaaggctatcgttgaac tcatcacacttcctcagctcgag
Scaffold.1	CipA-linker-CipC	ggtgtggtagtagaaattggcaaagttacgggatctgttggaactacagttgaaatacctgtatatttcagaggagttccatccaaaggaatagcaaactgcgactttgtgttcagat atgatccgaatgtattggaaattatagggatagatcccggagacataatagttgacccgaatcctaccaagagctttgatactgcaatatatcctgacagaaagataatagtattcct gtttgcggaagacagcggaacaggagcgtatgcaataactaaagacggagtatttgcaaaaataagagcaactgtaaaatcaagtgctccgggctatattactttcgacgaagta ggtggatttgcagataatgacctggtagaacagaaggtatcatttatagacggtggtgttaacgttggcaatgcaacaccgaccaagggagcaacaccaacaaatacagctacg ccgacaaaatcagctacggctacgcccaccaggccatcggtaccgacaaacacaccgacaaacacaccggcaaatacaccgggcagtgtagtaccatcaacacagcctgta acaacaccacctgcaacaacaaaaccacctgcaacaacaaaaccacctgcaacaacaatacccgccgtcagatgatccggggcgattctcttaaagttacagtaggaacagctaat ggtaagcctggcgatacagtaacagttcctgttacatttgctgatgtagcaaagatgaaaaacgtaggaacatgtaatttctatcttggatatgatgcaagcctgttagaggtagtatc agtagatgcaggtccaatagttaagaatgcagcagttaacttctcaagcagtgcaagcaacggaacaatcagcttcctgttcttggataacacaattacagacgaattgataactgc agacggtgtgtttgcaaatattaagttcaaattaaagagtgtaacggctaaaactacaacaccagtaacatttaaagatggtggagcttttggtgacggaactatgtcaaagatagct tcagttactaagacaaacggtagtgtaactatagatcctggtactcaa
Scaffold.2	CipA-linker- CBM-linker-CipC	ggtgtggtagtagaaattggcaaagttacgggatctgttggaactacagttgaaatacctgtatatttcagaggagttccatccaaaggaatagcaaactgcgactttgtgttcagat atgatccgaatgtattggaaattatagggatagatcccggagacataatagttgacccgaatcctaccaagagctttgatactgcaatatatcctgacagaaagataatagtattcct gtttgcggaagacagcggaacaggagcgtatgcaataactaaagacggagtatttgcaaaaataagagcaactgtaaaatcaagtgctccgggctatattactttcgacgaagta ggtggatttgcagataatgacctggtagaacagaaggtatcatttatagacggtggtgttaacgttggcaatgcaacaccgaccaagggagcaacaccaacaaatacagctacg ccgacaaaatcagctacggctacgcccaccaggccatcggtaccgacaaacacaccgacaaacacaccggcaaatacaccggtatcaggcaatttgaaggttgaattctacaa cagcaatccttcagatactactaactcaatcaatcctcagttcaaggttactaataccggaagcagtgcaattgatttgtccaaactcacattgagatattattatacagtagacggac agaaagatcagaccttctggtgtgaccatgctgcaataatcggcagtaacggcagctacaacggaattacttcaaatgtaaaaggaacatttgtaaaaatgagttcctcaacaaata acgcagacacctaccttgaaataagctttacaggcggaactcttgaaccgggtgcacatgttcagatacaaggtagatttgcaaagaatgactggagtaactatacacagtcaaat gactactcattcaagtctgcttcacagtttgttgaatgggatcaggtaacagcatacttgaacggtgttcttgtatggggtaaagaacccggtggcagtgtagtaccatcaacacagc ctgtaacaacaccacctgcaacaacaaaaccacctgcaacaacaaaaccacctgcaacaacaatacccgccgtcagatgatccggggcgattctcttaaagttacagtaggaacag ctaatggtaagcctggcgatacagtaacagttcctgttacatttgctgatgtagcaaagatgaaaaacgtaggaacatgtaatttctatcttggatatgatgcaagcctgttagaggta gtatcagtagatgcaggtccaatagttaagaatgcagcagttaacttctcaagcagtgcaagcaacggaacaatcagcttcctgttcttggataacacaattacagacgaattgata actgcagacggtgtgtttgcaaatattaagttcaaattaaagagtgtaacggctaaaactacaacaccagtaacatttaaagatggtggagcttttggtgacggaactatgtcaaaga tagcttcagttactaagacaaacggtagtgtaactatagatcctggtactcaactcgag
Scaffold.1 with SED1 anchor	CipA-linker- CBM-linker-CipC- SED1	ggtgtggtagtagaaattggcaaagttacgggatctgttggaactacagttgaaatacctgtatatttcagaggagttccatccaaaggaatagcaaactgcgactttgtgttcagat atgatccgaatgtattggaaattatagggatagatcccggagacataatagttgacccgaatcctaccaagagctttgatactgcaatatatcctgacagaaagataatagtattcct gtttgcggaagacagcggaacaggagcgtatgcaataactaaagacggagtatttgcaaaaataagagcaactgtaaaatcaagtgctccgggctatattactttcgacgaagta ggtggatttgcagataatgacctggtagaacagaaggtatcatttatagacggtggtgttaacgttggcaatgcaacaccgaccaagggagcaacaccaacaaatacagctacg ccgacaaaatcagctacggctacgcccaccaggccatcggtaccgacaaacacaccgacaaacacaccggcaaatacaccggtatcaggcaatttgaaggttgaattctacaa cagcaatccttcagatactactaactcaatcaatcctcagttcaaggttactaataccggaagcagtgcaattgatttgtccaaactcacattgagatattattatacagtagacggac agaaagatcagaccttctggtgtgaccatgctgcaataatcggcagtaacggcagctacaacggaattacttcaaatgtaaaaggaacatttgtaaaaatgagttcctcaacaaata acgcagacacctaccttgaaataagctttacaggcggaactcttgaaccgggtgcacatgttcagatacaaggtagatttgcaaagaatgactggagtaactatacacagtcaaat gactactcattcaagtctgcttcacagtttgttgaatgggatcaggtaacagcatacttgaacggtgttcttgtatggggtaaagaacccggtggcagtgtagtaccatcaacacagc ctgtaacaacaccacctgcaacaacaaaaccacctgcaacaacaaaaccacctgcaacaacaatacccgccgtcagatgatccggggcgattctcttaaagttacagtaggaacag ctaatggtaagcctggcgatacagtaacagttcctgttacatttgctgatgtagcaaagatgaaaaacgtaggaacatgtaatttctatcttggatatgatgcaagcctgttagaggta gtatcagtagatgcaggtccaatagttaagaatgcagcagttaacttctcaagcagtgcaagcaacggaacaatcagcttcctgttcttggataacacaattacagacgaattgata actgcagacggtgtgtttgcaaatattaagttcaaattaaagagtgtaacggctaaaactacaacaccagtaacatttaaagatggtggagcttttggtgacggaactatgtcaaaga tagcttcagttactaagacaaacggtagtgtaactatagatcctggtactcaactcgaggtggtggaggtagtggaggaggtggtagtcaattttccaacagtacatctgcttcttc caccgatgtcacttcctcctcttccatctccacttcctctggctcagtaactatcacatcttctgaagctccagaatccgacaacggtaccagcacagctgcaccaactgaaacctca acagaggctccaaccactgctatcccaactaacggtacctctactgaagctccaaccactgctatcccaactaacggtacctctactgaagctccaactgatactactactgaagct ccaaccaccgctcttccaactaacggtacttctactgaagctccaactgatactactactgaagctccaaccaccggtcttccaaccaacggtaccacttcagctttcccaccaact acatctttgccaccaagcaacactaccaccactcctccttacaacccatctactgactacaccactgactacactgtagtcactgaatatactacttactgtccagaaccaaccacttt

		caccacaaacggtaagacttacaccgtcactgaaccaaccacattgactatcactgactgtccatgcaccattgaaaagccaacaaccacatcaaccaccgaatacactgtagtc actgagtacactacttactgtccagaaccaaccactttcaccacaaacggtaagacttacaccgtcactgaaccaaccactttgactatcactgactgtccatgtactattgaaaaga gcgaagcccctgagtcttctgtcccagttaccgaatctaagggcactaccaccaaagaaacaggtgttactaccaaacaaaccacagccaacccaagtctaaccgtctccacag tcgtcccagtttcatcctctgcttcttctcattccgttgtcatcaacagtaacggtgctaacgtcgtcgttccaggtgctttaggtttggctggtgttgctatgttattcttataa
Scaffold.3	CipA-linker-CBM-linker-SH3$_D$	ggtgtggtagtagaaattggcaaagttacgggatctgttggaactacagttgaaatacctgtatatttcagaggagttccatccaaaggaatagcaaactgcgactttgtgttcagat atgatccgaatgtattggaaattatagggatagatcccggagacataatagttgacccgaatcctaccaagagctttgatactgcaatatatcctgacagaaagataatagtattcct gtttgcggaagacagcggaacaggagcgtatgcaataactaaagacggagtatttgcaaaaataagagcaactgtaaaatcaagtgctccgggctatattactttcgacgaagta ggtggatttgcagataatgacctggtagaacagaaggtatcatttatagacggtggtgttaacgttggcaatgcaacaccgaccaagggagcaacaccaacaaatacagctacg ccgacaaaatcagctacggctacgcccaccaggccatcggtaccgacaaacacaccgacaaacacaccggcaaatacaccggtatcaggcaatttgaaggttgaattctacaa cagcaatccttcagatactactaactcaatcaatcctcagttcaaggttactaataccggaagcagtgcaattgatttgtccaaactcacattgagatattattatacagtagacggac agaaagatcagaccttctggtgtgaccatgctgcaataatcggcagtaacggcagctacaacggaattacttcaaatgtaaaaggaacatttgtaaaaatgagttcctcaacaaata acgcagacacctaccttgaaataagctttacaggcggaactcttgaaccgggtgcacatgttcagatacaaggtagatttgcaaagaatgactggagtaactatacacagtcaaat gactactcattcaagtctgcttcacagtttgttgaatgggatcaggtaacagcatacttgaacggtgttcttgtatggggtaaagaacccggtggcagtgtagtaccatcaacacagc ctgtaacaacaccacctgcaacaacaaaaccacctgcaacaacaaaaccacctgcaacaacaatacccgccgtcagatgatccggaagaggcagaatatgttcgtgccctgtttg attttaatggcaacgatgaagaagatctgccgtttaaaaagggtgatattctgcgtattcgtgacaaaccggaagaacagtggtggaatgcagaagatagcgaaggtaaacgtgg tatgattccggttccgtatgttgaaaaatatcgtccg
Scaffold.4	CipA-linker-CBM-linker-SH3$_D$-ScaB	ggtgtggtagtagaaattggcaaagttacgggatctgttggaactacagttgaaatacctgtatatttcagaggagttccatccaaaggaatagcaaactgcgactttgtgttcagat atgatccgaatgtattggaaattatagggatagatcccggagacataatagttgacccgaatcctaccaagagctttgatactgcaatatatcctgacagaaagataatagtattcct gtttgcggaagacagcggaacaggagcgtatgcaataactaaagacggagtatttgcaaaaataagagcaactgtaaaatcaagtgctccgggctatattactttcgacgaagta ggtggatttgcagataatgacctggtagaacagaaggtatcatttatagacggtggtgttaacgttggcaatgcaacaccgaccaagggagcaacaccaacaaatacagctacg ccgacaaaatcagctacggctacgcccaccaggccatcggtaccgacaaacacaccgacaaacacaccggcaaatacaccggtatcaggcaatttgaaggttgaattctacaa cagcaatccttcagatactactaactcaatcaatcctcagttcaaggttactaataccggaagcagtgcaattgatttgtccaaactcacattgagatattattatacagtagacggac agaaagatcagaccttctggtgtgaccatgctgcaataatcggcagtaacggcagctacaacggaattacttcaaatgtaaaaggaacatttgtaaaaatgagttcctcaacaaata acgcagacacctaccttgaaataagctttacaggcggaactcttgaaccgggtgcacatgttcagatacaaggtagatttgcaaagaatgactggagtaactatacacagtcaaat gactactcattcaagtctgcttcacagtttgttgaatgggatcaggtaacagcatacttgaacggtgttcttgtatggggtaaagaacccggtggcagtgtagtaccatcaacacagc ctgtaacaacaccacctgcaacaacaaaaccacctgcaacaacaaaaccacctgcaacaacaatacccgccgtcagatgatccggaagaggcagaatatgttcgtgccctgtttg attttaatggcaacgatgaagaagatctgccgtttaaaaagggtgatattctgcgtattcgtgacaaaccggaagaacagtggtggaatgcagaagatagcgaaggtaaacgtgg tatgattccggttccgtatgttgaaaaatatcgtccgggatccgccggtggtttatccgctgtgcagcctaatgttagtttaggcgaagtactggatgtttctgctaacagaaccgctg ctgacggaacagttgaatggcttatcccaacagtaactgcagctccaggccagacggtcactatgcccgtagtagtcaagagttcaagtcttgcagttgctggtgcgcagttcaag atccaggcggcgacaggcgtacgttattcgtccaagacggacggtgacgcttacggttcaggcattgtgtacaataatagtaagtatgcttttggacagggtgcaggtagaggaa tagttgcagctgatgattcggttgtgcttactcttgcatatacagttcccgctgattgtgctgaaggtacatatgatgtcaagtggtctgatgcgtttgtaagtgatacagacggacaga atatcacaagtaaggttactcttactgatggcgctatcattgttaag
Primer	M1-F	ggaggctcaggaggtggaggctccggaggtggaggctcaggtggtggtagtacaccgct
Primer	M2-F	caccaaaaaggagaagatctggaggtggaggctcaggaggtggaggct
Primer	M3-F	catcatatgcctcctcctgctctgccaccaaaaaggagaagatct
Primer	M-R	gaattcggatccctcgagcggaggtgctgcacatgcaaaattg
Primer	Md-R	gcagagattacctatctagacggaggtgctgcacatgc
Primer	his-F	ggtaatacaccatgaatcacaaag
Primer	his-R	ctatctagagtggtggtggtggtggtggtcgacaagcttgaattcgg
Primer	pScf-F	cctcagatgggcagcagcggtaagcctatccctaaccctctcctc
Primer	pScf-R	gagaccttaattcgcttataagaataacatagcaacaccagc
Primer	pF-F	gacctcagatgggcagcagccatatgcagacaaatccctatgccc
Primer	pF-R	gtcagagagaccttaattcgctcacaagtcctcttcagaaatgagc
Primer	pM-F	ccatcagagacctcagatgggcagcagccatcatcatcatcatcacagc
Primer	pM-R	cagagagaccttaattcgctcagtggtggtggtggtggtgctcgag
Primer	pZM-F	ggcggccgccagcttacgtacatcatcatcatcatcacagcagcggcc
Primer	pZM-R	gtctaaggctacaaactcagtggtggtggtggtggtgctcgagttgg
Primer	pPIC9K-F	gcgaattaaggtctctctgacttagacatgactgttcctcagttcaag
Primer	pPIC9K-R	tgaggtctctgatggctgctgcccatgaattctacgtaagcttcagc
Primer	pPICZC-F	tgagtttgtagccttagacatgactgttcctcagttcaag
Primer	pPICZC-R	tacgtaagctggcggccgccgcggctcgaggtaccgatcc
Primer	qC-F	tcctgtttgcggaagacagcg
Primer	qC-R	tgttggtgttgctcccttggtc
Primer	qF-F	gtccgtttaccgtccgttct
Primer	qF-R	gcgctgtatagcctggaaca
Primer	qM-F	gcagaccacagtaacgacga
Primer	qM-R	cattgccgtctttcagtgcc
Primer	qGAPDH-F	gtggtcatcaaaccggactca
Primer	qGAPDH-R	caagaaggtcgtcatcactgctc

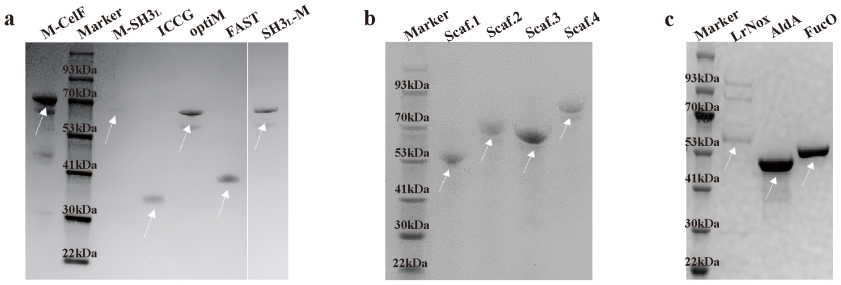

Supplementary Fig. 1: SDS-PAGE of purified recombinant enzymes and protein scaffolds used in this study. SDS-PAGE analysis of purified proteins stained with Coomassie Blue. **a** M-CelF: MHETase-CelF; optiM: codon optimized MHETase; M-SH3$_L$: optiMHETase-SH3$_L$; SH3$_L$-M: SH3$_L$-optiMHETase; ICCG: ICCG-ScaA; FAST: FAST-PETase-CelF. **b** Scaf.1: CipA-CipC; Scaf.2: CipA-CBM-CipC; Scaf.3: CipA-CBM-SH3$_D$; Scaf.4: CipA-CBM-SH3$_D$-ScaB. **c** LrNox: LrNox-ScaA; FucO: FucO-CelF; AldA: SH3$_L$-AldA.

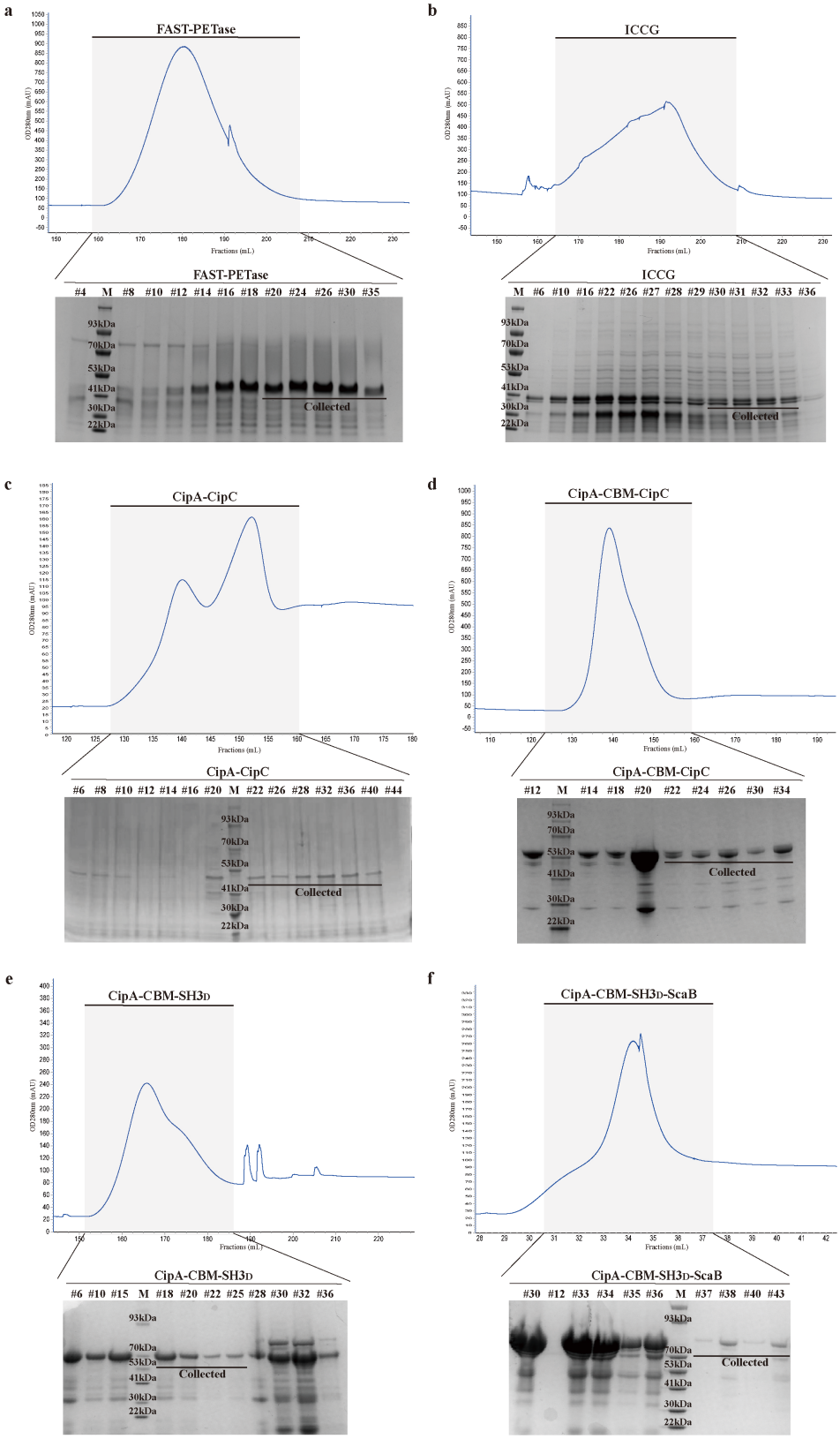

Supplementary Fig. 2: Purification profiles of key enzymes and scaffolds. a-f FPLC chromatograms (top) and corresponding SDS-PAGE analysis of elution fractions (bottom) for His-tag purified proteins. Shaded regions on chromatograms indicate the elution fractions from the HisTrap column subjected to SDS-PAGE analysis. **a** FAST-PETase-CelK. **b** ICCG-ScaA. **c** CipA-CipC (Scaf.1). **d** CipA-CBM-CipC (Scaf.2). **e** CipA-CBM-SH3$_D$ (Scaf.3). **f** CipA-CBM-SH3$_D$-ScaB (Scaf.4). M, protein molecular weight marker.

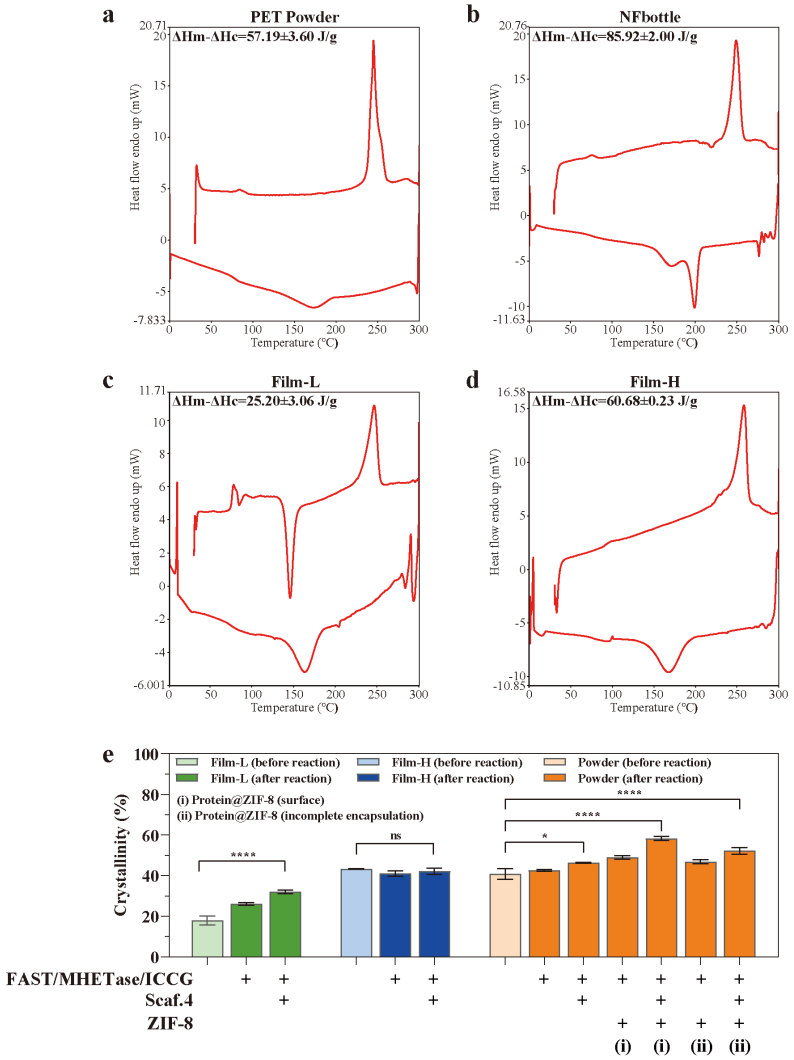

Supplementary Fig. 3: Crystallinity characterization of PET substrates. Differential scanning calorimetry (DSC) thermograms used to determine the crystallinity of PET substrates used in this study. **a** PET powder (40.82%). **b** Commercial water bottle (NFbottle, 61.33%). **c** Film-L (17.99%). **d** Film-H (43.31%). ΔHm, heat of melting; ΔHc, heat of cold crystallization. **e** Comparison of substrate crystallinity before and after a 96-h reaction with optiComplex-D or immobilized complexes at 40 °C, pH 7.0, using 100 mg PET substrate, 0.25 nmol individual enzymes, with an enzyme:scaffold molar ratio of 0.5:1. The apparent increase in crystallinity post-reaction is a known phenomenon; it occurs because the enzymes preferentially degrade the more accessible amorphous regions, thereby enriching the proportion of crystalline domains in the remaining material. Data are presented as mean ± s.d. (n = 3). Statistical significance was determined by one-way ANOVA (ns: not significant, *p < 0.1, **p < 0.01, ***p < 0.001, ****p < 0.0001).

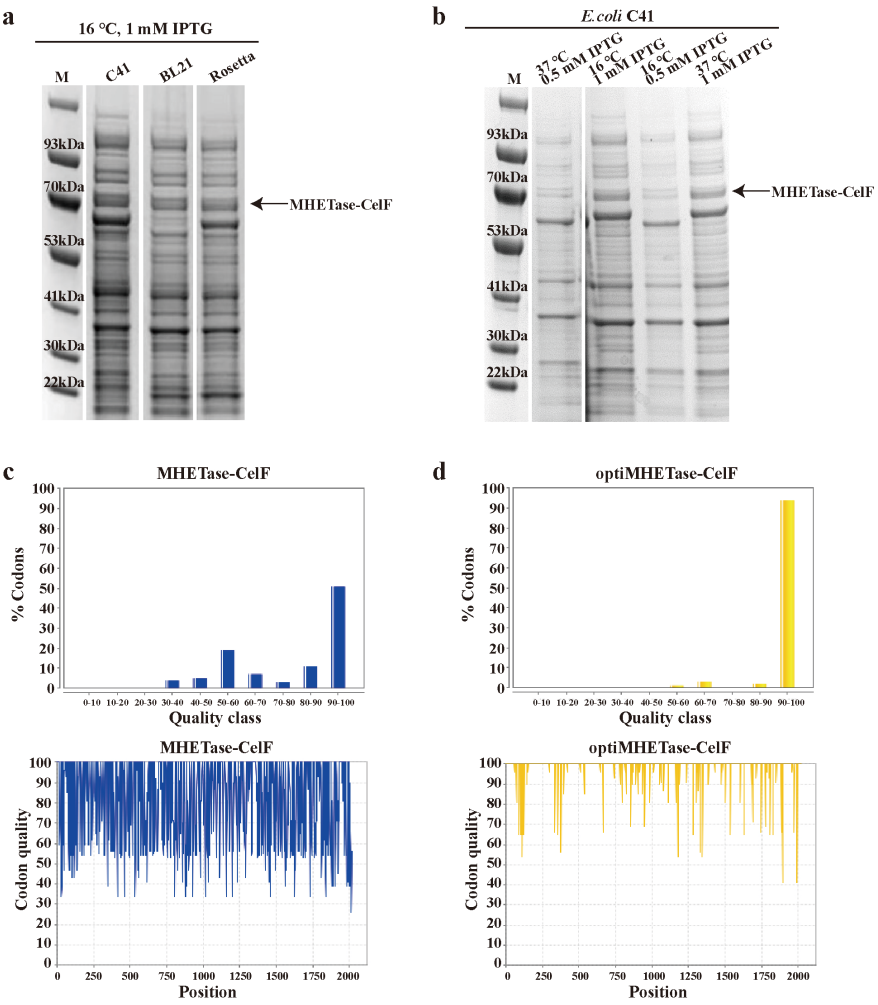

Supplementary Fig. 4: Optimization of MHETase expression in *E. coli*. a Screening of different *E. coli* expression strains, identifying C41(DE3) as the most effective host. **b** Optimization of induction temperature and isopropyl β-D-1-thiogalactopyranoside (IPTG) concentration in the C41(DE3) strain. Optimal expression was achieved at 16 °C with 1 mM IPTG for 18 h. M, protein molecular weight marker. The optimized expression condition was confirmed using *E. coli* C41 (DE3) for 12 hours at 16°C, with the addition of 1 mM IPTG for the induction. **c**, **d** Codon usage analysis before (**c**) and after (**d**) codon optimization for *E. coli* expression. The optimized gene shows a significantly improved distribution of high-quality codons (90-100 quality class). Results were calculated by GeneArt™ GeneOptimizer™ (Thermo Fisher).

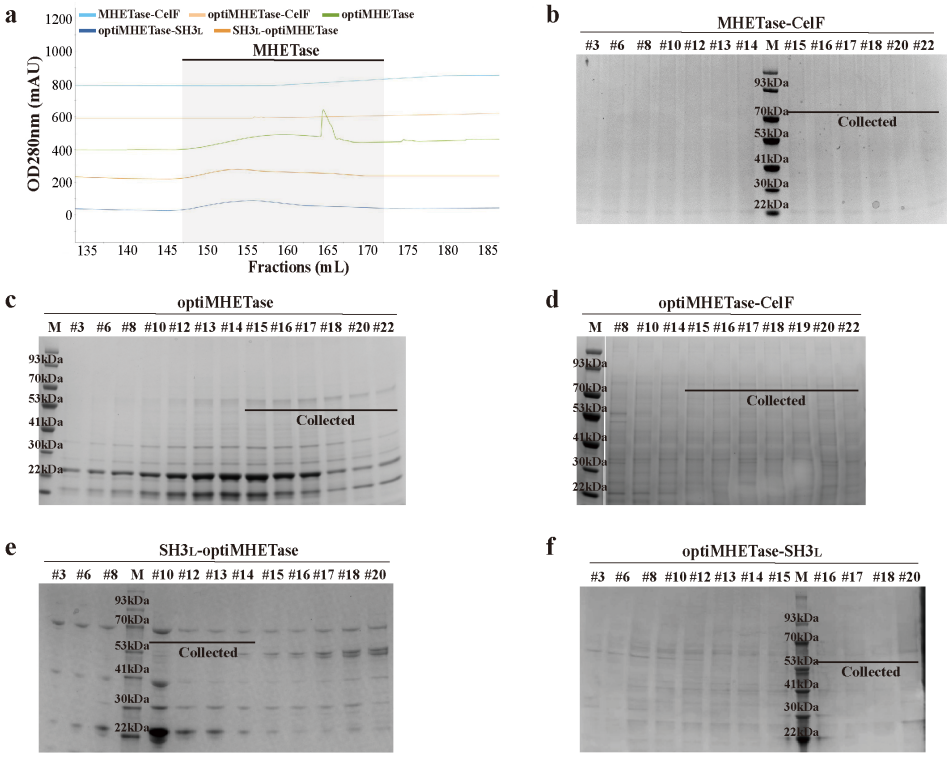

Supplementary Fig. 5: Purification profiles for MHETase variants. a Overlay of FPLC chromatograms for different MHETase constructs purified via His-tag affinity chromatography. **b-f** SDS-PAGE analysis of elution fractions for each construct, confirming the purity of the collected fractions (indicated by black bars).

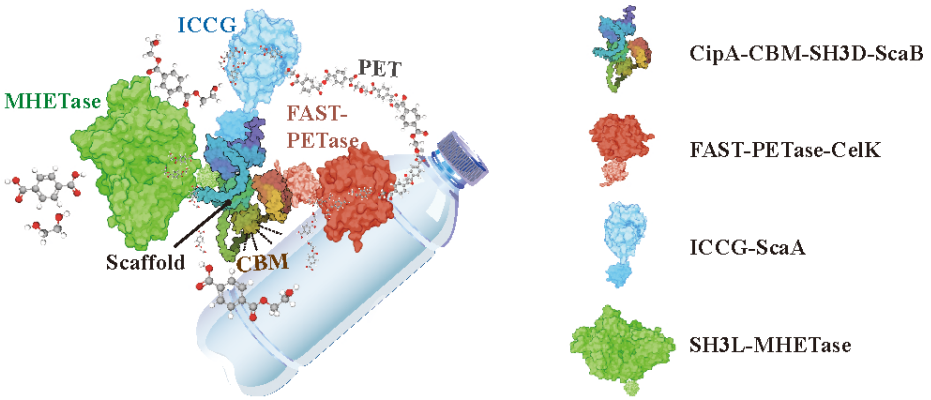

Supplementary Fig. 6: Structural model of the three-enzyme Complex-D. A model of the fully assembled complex, generated by integrating experimentally determined structures of the enzymes with an AlphaFold2-predicted structure of the Scaf.4 scaffold. Individual components are shown on the right for clarity.

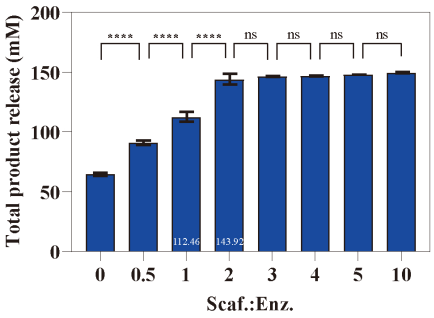

Supplementary Fig. 7: Effect of enzyme-to-scaffold molar ratio on Complex-D activity. PET degradation assays were performed with a fixed concentration of enzymes (0.25 nmol each of FAST, optiMHETase, ICCG) and varying concentrations of Scaf.4. The data show that activity plateaus at a scaffold:enzyme molar ratio of approximately 2:1, indicating saturation of the enzymes with scaffold. Reactions used 100 mg PET powder at 30 °C, pH 7.0, for 96 h. Data are presented as mean ± s.d. (n = 3). Statistical significance was determined by one-way ANOVA (ns: not significant, *$p < 0.1$, **$p < 0.01$, ***$p < 0.001$, ****$p < 0.0001$).

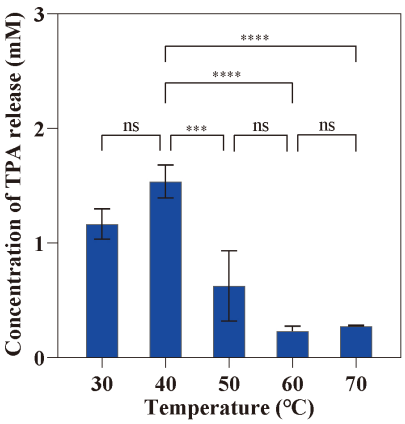

Supplementary Fig. 8: Effect of temperature on $SH3_L$-optiMHETase activity. Activity of SH3L-optiMHETase was assayed on a mixture of 5 mM MHET and BHET at different temperatures with 0.5 μM enzyme at pH 7.0 for 96 h. The enzyme shows the highest activity for converting intermediates to TPA at 40 °C, consistent with the optimal temperature determined for the complete Complex-D cascade. The elevated TPA release observed in the 70 °C group was likely attributed to the self-degradation of the monomers under high temperatures. Data are presented as mean ± s.d. (n = 3). Statistical significance was determined by one-way ANOVA (ns: not significant, *$p < 0.1$, **$p < 0.01$, ***$p < 0.001$, ****$p < 0.0001$).

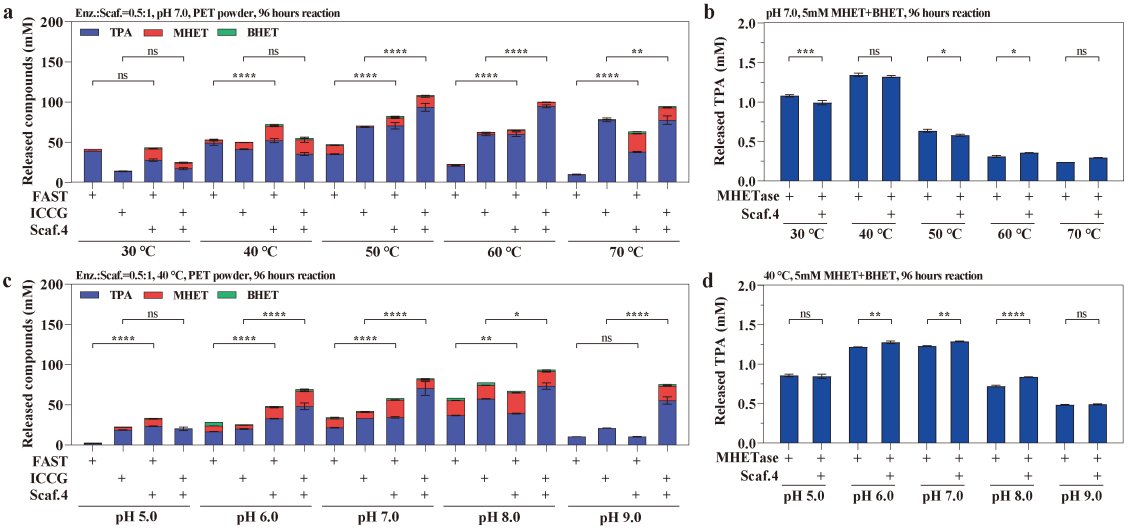

Supplementary Fig. 9: Comparison of scaffolded and free enzyme performance across varying pH and temperature conditions. Degradation of PET powder or intermediates MHET and BHET by the scaffolded enzymes was compared to an equimolar mixture of the corresponding free enzymes. **a-b** Temperature profile showing total product release across a range of temperatures (30-70°C) at pH 7.0. **c-d** pH profile showing total product release across a range of pH values (5.0-9.0) at 40°C. All reactions were performed for 96 hours using 100 mg PET powder or 5 mM MHET and BHET, using 0.25 nmol individual enzymes. Data are presented as mean ± s.d. (n = 3). Statistical significance was determined by one-way ANOVA (ns: not significant, *p < 0.1, **p < 0.01, ***p < 0.001, ****p < 0.0001).

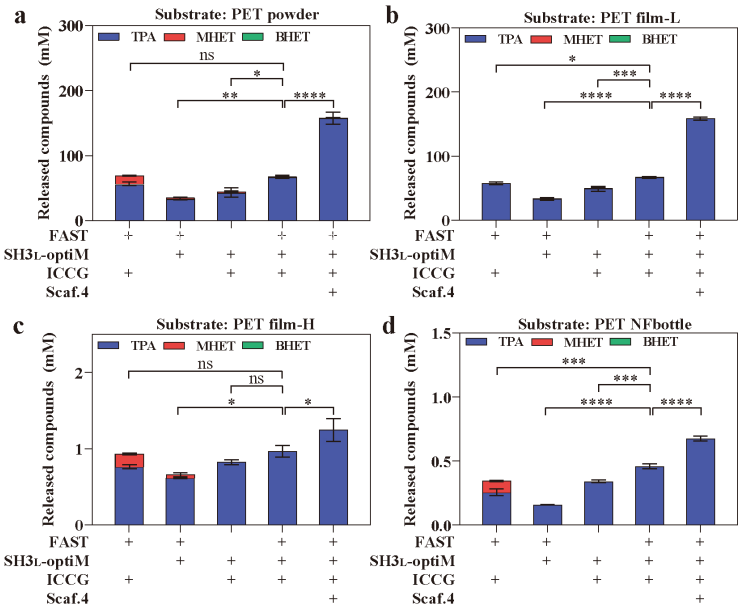

Supplementary Fig. 10: Performance of optiComplex-D across diverse PET substrates. Degradation assays under optimal reaction conditions (40 °C, pH 7.0, 96 h) comparing non-scaffolded enzyme mixtures with the fully assembled optiComplex-D. The scaffolded complex consistently shows superior performance on **a**, PET powder, **b**, low-crystallinity film (film-L), **c**, high-crystallinity film (film-H), and **d**, a commercial water bottle (NFbottle). All reactions contain 100 mg PET substrate, 0.25 nmol individual enzymes, with an enzyme:scaffold molar ratio of 0.5:1. Data are presented as mean ± s.d. (n = 3). Statistical significance was determined by one-way ANOVA (ns: not significant, *$p < 0.1$, **$p < 0.01$, ***$p < 0.001$, ****$p < 0.0001$).

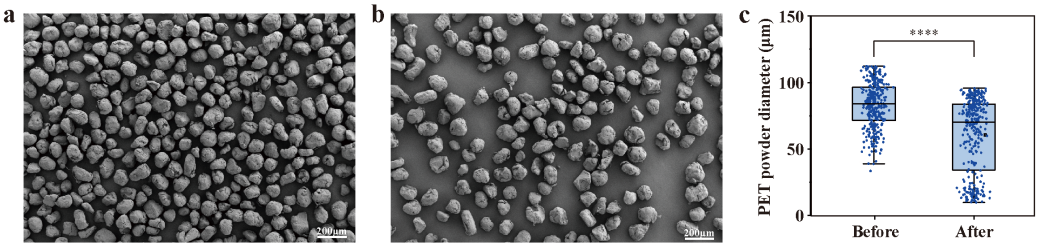

Supplementary Fig. 11: Enzymatic treatment reduces PET powder particle size. a, **b** SEM images of PET powder before (**a**) and after (**b**) a 96 h treatment with optiComplex-D at 40 °C, pH 7.0. **c** Boxplot analysis quantifying the significant decrease in particle diameter after enzymatic degradation. The box extends from the 25th to 75th percentiles, the line indicates the median, and whiskers show the min to max range. Statistical significance was determined by one-way ANOVA (****$p < 0.0001$).

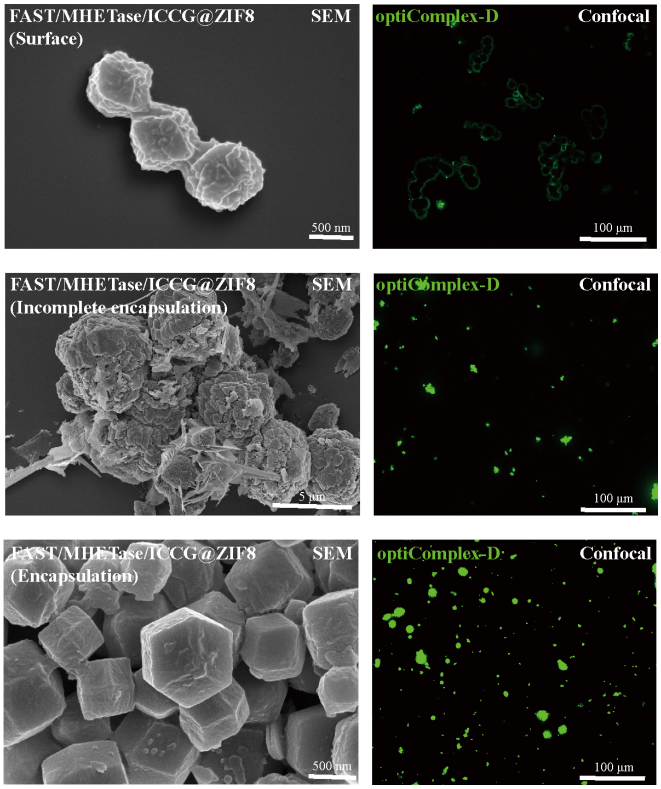

Supplementary Fig. 12: Characterization of non-scaffolded enzymes immobilized on ZIF-8. SEM and confocal microscopy images of a mixture of free enzymes (FAST-PETase, MHETase, and ICCG) immobilized on ZIF-8 using the three different strategies (surface, incomplete encapsulation, encapsulation), corresponding to the controls used in **Fig. 5**. His-tagged proteins were detected with an Alexa Fluor® 488 conjugated anti-His antibody. The loading efficiency of FAST/MHETase/ICCG@ZIF-8 was 78.11% (surface), 93.99% (incomplete encapsulation), and 90.14% (encapsulation). Confocal images serve as qualitative confirmation of successful immobilization; variations in fluorescence intensity are not for quantitative comparison of enzyme loading.

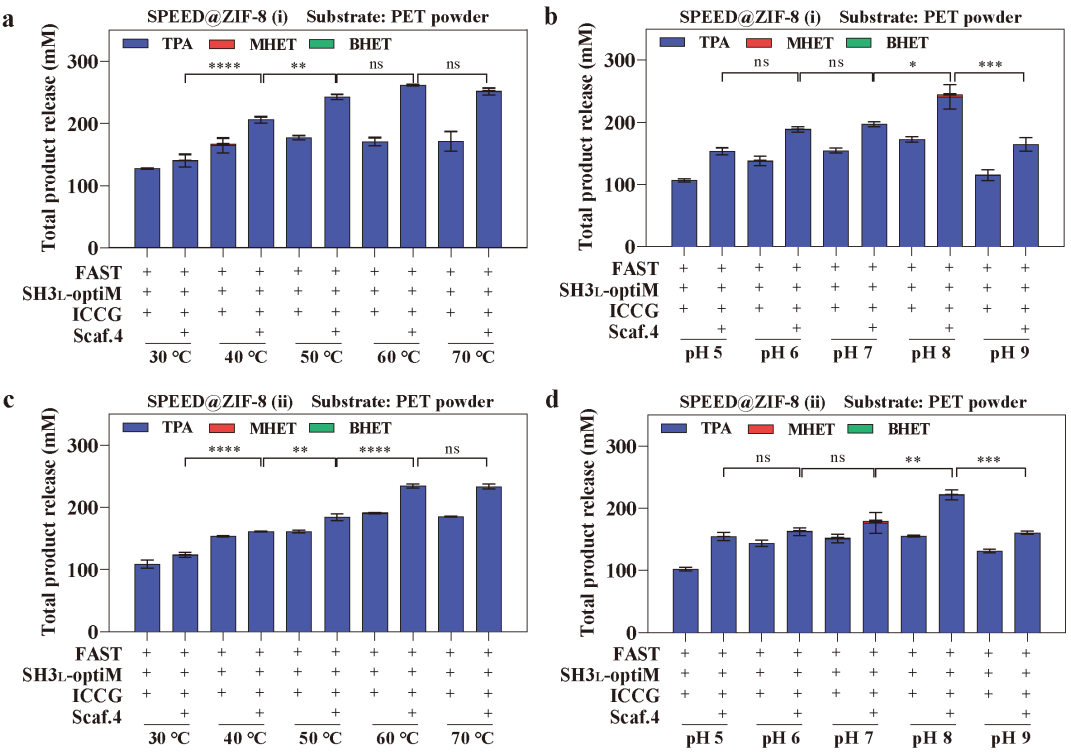

Supplementary Fig. 13: ZIF-8 immobilization broadens the operational window of optiComplex-D. Temperature (**a, c**) and pH (**b, d**) stability profiles for optiComplex-D immobilized on the surface of ZIF-8 (**a, b**) or via incomplete encapsulation (**c, d**). Compared to the free enzyme (**Fig. 4**), immobilization confers enhanced stability, particularly at higher temperatures. Reactions were performed with 100 mg PET powder, 0.25 nmol enzymes in a 0.5:1 enzyme:scaffold ratio for 96 h. The residual activity observed at low pH may be attributed to partial enzyme release from the ZIF-8 matrix under acidic conditions[64,65]. Data are presented as mean ± s.d. (n = 3). Statistical significance was determined by one-way ANOVA (ns: not significant, *$p < 0.1$, **$p < 0.01$, ***$p < 0.001$, ****$p < 0.0001$).

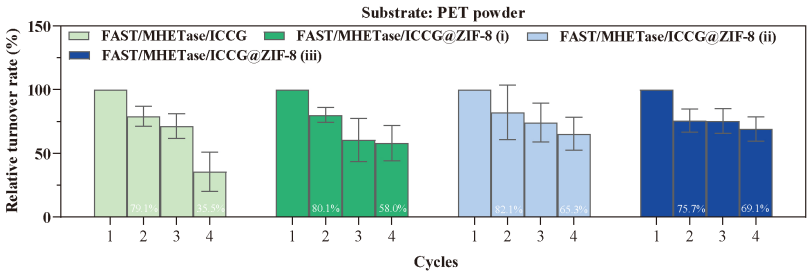

Supplementary Fig. 14: Reusability of ZIF-8 immobilized non-scaffolded enzymes. Relative activity of free and immobilized non-scaffolded enzyme mixtures (FAST/MHETase/ICCG) over four 4-day reaction cycles. Immobilization improves reusability compared to the free enzymes, but performance is inferior to the scaffolded complexes shown in **Fig. 5d**. Reactions were performed at 40 °C, pH 7.0 with 100 mg PET powder, 0.25 nmol individual enzymes. Data are presented as mean ± s.d. (n = 3).

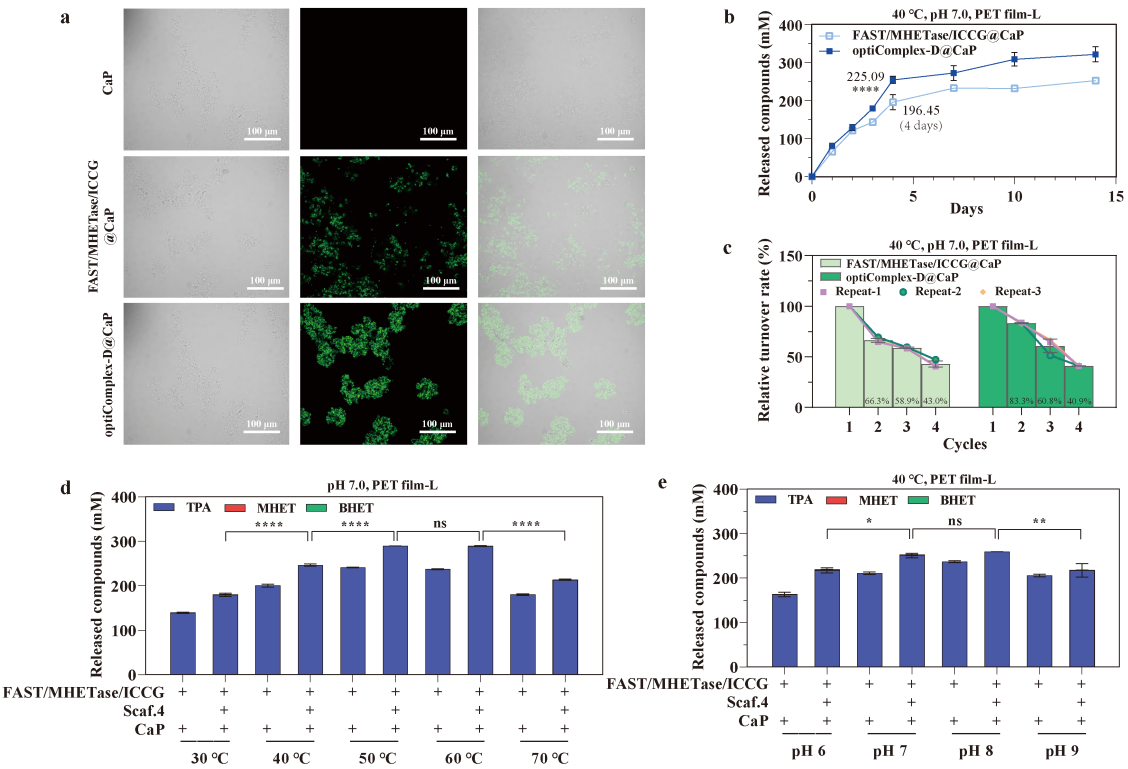

Supplementary Fig. 15: Performance of optiComplex-D immobilized on calcium phosphate (CaP). a Confocal microscopy images confirming successful immobilization of scaffolded (optiComplex-D) and non-scaffolded enzymes on CaP crystals. Alexa Fluor® 488 conjugated anti-His antibody was used to detect His-tagged proteins. The loading efficiency of FAST/MHETase/ICCG and optiComplex-D on CaP was 83.20% and 79.95%, respectively. **b** Long-term (14-day) time-course PET degradation analysis, showing an improvement over free enzyme complex. **c** Reusability over four 4-day cycles. FAST/MHETase/ICCG, a mixture of FAST-PETase, ICCG, and MHETase (0.25 nmol of each). **d**, **e** Temperature (**d**) and pH (**e**) stability profiles, demonstrating that CaP provides limited thermal and acid stability compared to ZIF-8 (**Supplementary Fig. 12**). Reactions were performed with 100 mg PET film-L using 0.5:1 enzyme:scaffold ratio. Data are presented as mean ± s.d. (n = 3). Statistical significance was determined by one-way ANOVA (ns: not significant, *p < 0.1, **p < 0.01, ***p < 0.001, ****p < 0.0001.)

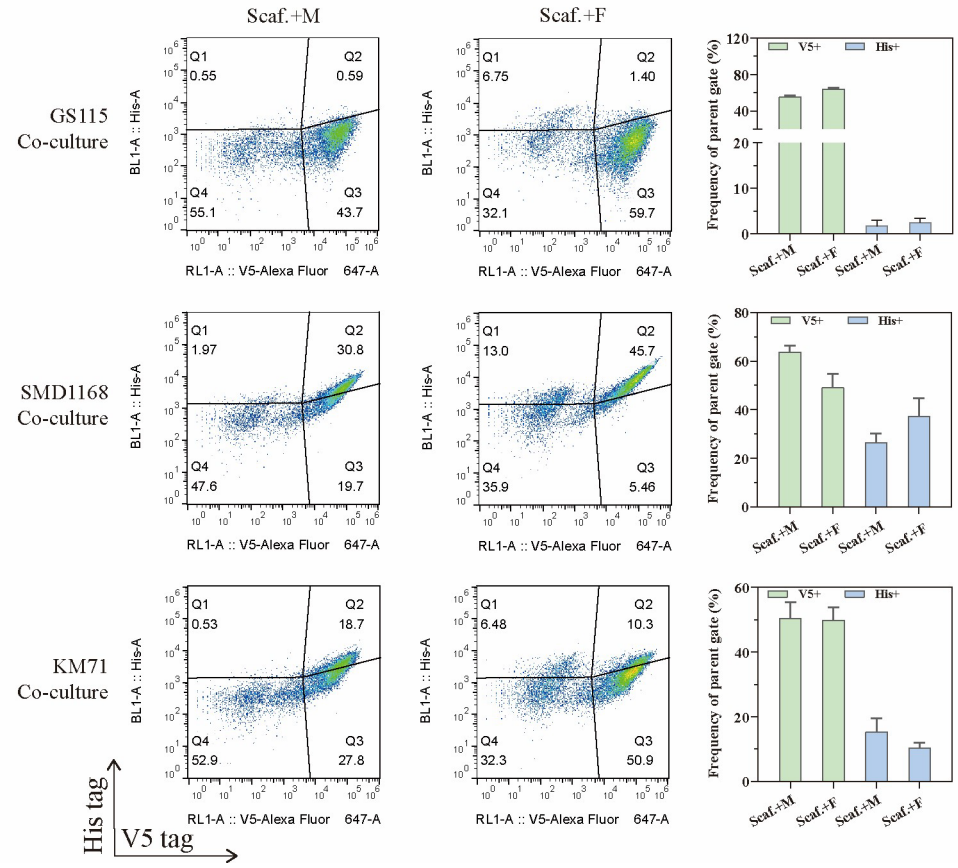

Supplementary Fig. 16: Screening of *P. pastoris* strains for scaffold expression and enzyme secretion. Flow cytometry analysis of co-cultures of V5-tagged scaffold-displaying and His-tagged enzyme-secreting yeast at 30°C in BMMY medium. Three different *P. pastoris* host strains (GS115, SMD1168, KM71) were tested. Each co-culture consisted of a scaffold-displaying strain (Scaf.; His4::CipA-CBM-CipC-SED1) mixed at a 1:1 ratio with either an MHETase-secreting strain (M; His4::MHETase) or a FAST-secreting strain (F; His4::FAST). The SMD1168 strain showed the highest percentage of cells positive for both scaffold display and enzyme binding (co-localization), and was therefore selected for the experiments in **Fig. 7**.

Supplementary Methods

Calculation of total enzyme molar amount

To facilitate a standardized comparison across different studies, the total molar amount of enzymes used in each reaction was calculated. Initial data, including either the mass or concentration of each enzyme, were extracted from the corresponding publications (**Supplementary File 1**). The total enzyme amount was determined by summing the molar amounts of the individual enzymes involved in each reported system. The molar amount for a single enzyme was calculated based on one of the following two scenarios:

1. For studies reporting enzyme mass, the molar amount was calculated as:

$$Molar\ amount\ of\ single\ enzyme\ (nmol) = \frac{Weight\ (\mu g)}{Molecular\ weight\ (kDa)}$$

The molecular weight of each enzyme was determined using the ExPASy ProtParam tool.

2. For studies reporting enzyme concentration, the molar amount was calculated as:

$$Molar\ amount\ of\ single\ enzyme\ (nmol) = \frac{Concentration\ (nM) \times Volume\ (mL)}{1000}$$

Calculation of total product molar amount

The total molar amount of degradation products (including TPA, EG, MHET, and BHET) was determined from product concentration or substrate mass loss data reported in the referenced literature (**Supplementary File 1**).

1. When product concentrations were provided, the total molar amount was calculated as:

$$Molar\ amount\ of\ total\ products\ (\mu mol) = Concentration(mM) \times Volume(mL)$$

2. When substrate mass loss was provided, the total molar amount was calculated as:

$$Molar\ amount\ of\ total\ products\ (\mu mol) = \frac{Weight\ loss\ (\%) \times Weight\ of\ PET\ (mg) \times 10}{192}$$

where 192 g/mol is the molecular weight of the polyethylene terephthalate (PET) repeating unit.

Calculation of degradation efficiency

To normalize catalytic performance, degradation efficiency was calculated as the total moles of product generated per mole of enzyme used.

$$Degradation\ efficiency\ (mol/mmol) = \frac{Molar\ amount\ of\ total\ products\ (\mu mol)}{Molar\ amount\ of\ single\ enzyme\ (nmol)}$$

Calculation of monomer conversion fidelity

The efficiency of converting intermediates into the final recyclable monomers was assessed by calculating the percentage of monomer release. This metric reflects the fidelity of the multi-enzyme cascade.

$$Recyclable\ monomer\ release\ (\%) = \frac{Concentration_{TPA+EG}\ (mM)}{Concentration_{TPA+EG+MHET+BHET}\ (mM)} \times 100\%$$

Calculation of PET conversion extent

The extent of PET substrate conversion was calculated based on the total molar amount of soluble degradation products (TPA, MHET, BHET) quantified by HPLC. The conversion percentage was

determined using the following formula:

$$PET\ weight\ loss\ (mg) = 5 \times 10^{-4} \times ((166 + 62) \times C_{TPA} + 210 \times C_{MHET} + 254 \times C_{BHET})$$

$$PET\ conversion\ extent\ (\%) = \frac{PET\ weight\ loss\ (mg)}{100\ (mg)} \times 100\%$$

where C_{TPA}, C_{MHET}, C_{BHET} are the molar concentrations (mol/L) of TPA, MHET, and BHET, respectively. Note that EG has equal molar amount to TPA.